Arrested versus active silica diagenesis reaction boundaries — A review of seismic diagnostic criteria

Shahab Varkouhi[1,3], Joseph A. Cartwright[1], Nicholas J. Tosca[2], Dominic Papineau[3]

1 Department of Earth Sciences, University of Oxford, Oxford, UK

2 Department of Earth Sciences, University of Cambridge, Cambridge, UK

3 Department of Earth Sciences, University College London, London, UK

Abstract

This paper evaluates previously proposed diagnostic criteria that can be used to determine whether or not there is active migration of the opal-A to opal-CT transition zone ($TZ_{A/CT}$). The criteria are based on the interpretation of 2D and 3D seismic surveys, and are therefore geometrical. They involve an assessment of the relationship of the $TZ_{A/CT}$ with polygonal fault systems, differential compaction structures, and tectonic folds. The most robust evidence for an inactive 'reaction front' between opal-A and opal-CT bearing sediments is the discordance of the $TZ_{A/CT}$ relative to present-day isotherms. Any of these may be persuasive as diagnostic criteria for the upward arrest of the diagenetic transformation at a regional scale, but actual truncation of the $TZ_{A/CT}$ at the modern seabed is definitive for arrested diagenesis. This study argues that diagenetic assessment based solely on a single criterion independently is not reliable as an indicator for the current state of a silica transition. As a conclusion, the analysed seismic/structural criteria should be synthesised to provide a more credible interpretation for silica diagenesis. The use of modern 2D and 3D seismic data for the reconstruction of the diagenetic history of opaline silica bearing sediments offers a new approach to the study of silica diagenesis at a regional scale.

Keywords: Silica diagenesis; bottom simulating reflector; seismic stratigraphy; differential compaction folding; polygonal fault systems

1. Introduction

The transformation of silica from opal-A (biogenic opal) to opal-CT (cristobalite/tridymite) is the most conspicuous diagenetic event present in modern and ancient deep-sea sediments where diatomaceous oozes are major constituents of ocean basin floors. This transformation comprises a complex set of dissolution–reprecipitation reactions (Stein and Kirkpatrick, 1976;

Kastner et al., 1977; Leeder, 1982; Williams and Crerar, 1985; Williams et al., 1985; Wrona et al., 2017a), which lead to marked changes in the host sediment petrophysics, particularly a porosity drop (Isaacs, 1981; Tada, 1991; Nobes et al., 1992; Chaika and Dvorkin, 1997, 2000; Meadows and Davies, 2007, 2009; Weller and Behl, 2015). These petrophysical variations are essentially due to extensive dissolution of opal-A and lesser impacts from precipitation of pore-filling opal-CT (Wrona et al., 2017a; Wrona et al., 2017b; Wrona et al., 2017c; Varkouhi et al., 2020a; Varkouhi et al., 2020b). A marked reduction in the content of biosilica frustules following dissolution significantly reduces the sediment stability, which makes its framework susceptible to abrupt collapse, sharp reduction in intergranular and intragranular porosities, and an appreciable interstitial-water expulsion (Varkouhi et al., 2020a; Varkouhi et al., 2020b). A lesser role for subsequent formation of diagenetic opal on physical-property response than pioneer dissolution of biogenic opal is commonly due to the restraining influences of authigenic phases other than opal-CT (e.g. authigenic clays) that precipitate mostly concomitant with silica diagenesis and restrict substantial formation of opal-CT through affecting the solubility and chemical kinetics of pore-water silica (Emerson and Hedges, 2008; Loucaides et al., 2010; Varkouhi and Wells, 2020; Varkouhi et al., 2020b; Varkouhi et al., 2021). The prominent increase in sediment bulk density over a vertical extent of a few metres results from porosity reduction, and compressional velocity increases owe to cementation of pore space by opal-CT (Varkouhi et al., 2020a). As a result, acoustic impedance dramatically increases, allowing these petrophysical changes to be imaged on seismic profiles as a high-amplitude discrete reflection or composite reflection that is most easily identified when it exhibits a discordant geometry with the host stratigraphy (Brekke, 2000; Davies and Cartwright 2002; Davies, 2005; Davies et al., 2009; Ireland et al., 2010; Neagu et al., 2010a; Neagu et al., 2010b).

This high amplitude reflection is found to crudely mark the position of a transition zone, where opal-A is gradually lost, and replaced by opal-CT (hereafter $TZ_{A/CT}$). The mapping and interpretation of the $TZ_{A/CT}$ is important for a general understanding of petroleum systems (Perrodon et al., 1998; Davies and Cartwright, 2002; Dralus et al., 2015), as a major drilling hazard (presence of hard sub-seabottom porcellaneous and chert layers containing opal-CT; Neagu, 2011; Roberts, 2014), and more fundamentally to place the significance of silica diagenesis in a basin evolutionary context (Davies, 2005; Wrona et al., 2017a).

Research into biogenic silica diagenesis in deep-water deposits is a broad theme that has been based on seismic reflection profiling (for a review of the literature, see Cartwright, 2007), scientific drillings (see Neagu, 2011 for a literature review), and outcrop examinations (see Chaika, 1998). The $TZ_{A/CT}$ was first recognised on 2D seismic reflection profiles acquired during research cruises linked to the earliest drilling campaigns of the Deep Sea Drilling Project (DSDP) (Hein et al., 1978; Lonsdale, 1990). These early investigations were focused on Late Cenozoic deep-sea sediments deposited on lower continental slopes of the southern Bering Sea, where the seismic reflection from the $TZ_{A/CT}$ was parallel to the modern seafloor. As a result, the diagenetic reflection was commonly described as a bottom simulating reflector (BSR)—a distinct reflection that roughly parallels the seabed based on seismic reflection images that exhibit high-amplitude reverse-polarity waveforms (Dillon et al., 1993; Sheriff and Geldart, 1995; Hillman et al., 2017; Ohde et al., 2018). Silica diagenesis was further researched over the past three decades, largely catalysed by the drilling campaigns of Ocean Drilling Program (ODP), which involved both 2D and 3D mapping of the $TZ_{A/CT}$ and its sediment sampling (after Neagu, 2011; Varkouhi, 2018. Also see Ocean Drilling Program Publication Services, 2012). The $TZ_{A/CT}$ has been also described from biosiliceous sedimentary rocks on land. The most extensive and well-researched outcrops being from the Miocene Monterey Formation in California, where the diagenesis of soft diatomaceous oozes has resulted in the development of significant hydrocarbon reservoirs in diagenetically formed tight chert and diatomite (Pisciotto, 1981; Isaacs, 1981, 1982; Keller and Isaacs, 1985; Behl and Garrison, 1994; Chaika, 1998; Chaika and Williams, 2001).

One of the most unresolved questions in silica diagenetic research is the recognition and study of arrested transition zones as opposed to currently active $TZ_{A/CT}$. Deciphering the diagenetic state of $TZ_{A/CT}$, i.e. arrested or active transition zone, is critical for a better understanding of biogenic silica diagenesis (Neagu et al., 2010b) and for reconstructing the thermal history of sediments hosting this diagenetic reaction (Pisciotto, 1981; Pisciotto et al., 1992; Wrona et al. 2017a; Varkouhi, 2018; Varkouhi et al., 2021). By 'arrested' (also referred to as fossilised by Davies and Cartwright, 2002; Neagu et al., 2010b), this study means the transition across which transformation from opal-A to opal-CT is presently static; implying that the regional transition zone is not currently at or near the phase stability boundary between opal-A and opal-CT. The arrested status of diagenesis is determined from certain specific stratigraphic and structural relationships between the reaction front and the host sediments (Davies and Cartwright, 2002). These relationships imply that the silica front is unlikely to be active in its current sub-seafloor position. Importantly, the lack of equilibrium with the present-day temperature field in the basin is considered the main clue that accounts for the arrested state of the $TZ_{A/CT}$ and therefore its discordant attitude relative to the present-day seabed, i.e.

a non bottom simulating reflector (non-BSR) (Brekke, 2000; Fig. 1A). The disequilibrium leading to arrested transitions has been attributed to a marked reduction in the thermal regime of the host basin in the recent past (Brekke, 2000; Neagu et al., 2010b). Conversely, silica diagenesis is still ongoing across active transitions. The long established view of an active $TZ_{A/CT}$, being geometrically close to seabottom simulating was developed based on the discordant basin-wide stratigraphic relationships between the $TZ_{A/CT}$ and its host strata (Hein et al., 1978; Lonsdale, 1990; Fig. 1B).

In the past four decades, several studies have proposed interpretational criteria which allow a distinction to be made between arrested and active transition zones on a case by case basis (Table 1). These criteria are based on seismic structural examination of the $TZ_{A/CT}$ and mostly support the notion of presently arrested transitions. However, it should be noted that the seismic reflection that is interpreted as the diagenetic front is not able to reveal the subtle variations in composition that really define the $TZ_{A/CT}$ (Varkouhi, 2018; Varkouhi et al., 2020b). Geochemical data, including pore-water saturation state with respect to silica polymorphs can provide added constraints to the seismic interpretations (Varkouhi et al., 2020b). However, such supplemental evidence for the dissolution kinetics of amorphous opal and precipitation of diagenetic silica is at the pore-water sample scale, and cannot be easily translated to modelling of migration of the opal-A to opal-CT reaction front at a regional scale. The precision of a seismic stratigraphic approach is further challenged by Meadows and Davies (2007) who discussed the morphologies of the silica front cross-sectional morphologies in the Sea of Okhotsk. According to their study, though a discordant feature relative to the modern seabed, the reaction over the $TZ_{A/CT}$ would not cease completely (the arrested condition), and they argue instead that there has been a dramatic decrease in the opal-A to opal-CT transformation rate in the final stage of basin evolution.

Given the significance of determining the diagenetic state of the $TZ_{A/CT}$, the principal aim of this paper is to review the seismic criteria developed by earlier research (compiled in Table 1) to differentiate arrested versus active silica diagenesis transition zones. The intention here is not to exhaustively discuss these interpretational criteria, but to critically examine their reliability and to provide insights, drawn based on the use of these criteria by former works, into the potential of seismic stratigraphy method for silica diagenetic research.

2. Diagenetic criteria – Review and assessment

2.1. Geometrical relationship to present-day isotherms

Roaldset and He (1995) were the first who proposed that disequilibrium with present-day temperature structure supports the view of a presently arrested $TZ_{A/CT}$ within Neogene deposits in the Barents Sea. Brekke (2000) and Neagu et al. (2010b) further argued for this criterion for the $TZ_{A/CT}$ in the Atlantic mid-Norwegian margin sediments by linking the cause of regionally discordant attitude of this transition zone relative to the present-day isotherms, including those at the seafloor to the arrested diagenesis (Fig. 2). Meadows and Davies (2007), in contrast, discuss the $TZ_{A/CT}$ hosted within the Miocene deposits from the Sea of Okhotsk as an example of a discordant-to-modern seabed feature that is likely to represent active silica diagenesis, notwithstanding its parallel relationship to the overlying Late Miocene Unconformity (Fig. 3). They suggest that the $TZ_{A/CT}$ was ascending through the sediments parallel to the isotherms at this time (Late Miocene), and that its sluggish behaviour after the Late Miocene is likely due to erosion of overburden or an increase in sedimentation rates relative to the rate of silica diagenetic reactions. Although the present stratigraphic architecture is not able to distinguish between these mutually exclusive possibilities, an episode of Late Pliocene basin inversion which led to the deformation of pre-existing structures suggests a more role for the overburden erosion on significant reduction in the rate of opal-A to opal-CT transformation across the $TZ_{A/CT}$ from the Sea of Okhotsk than the influence of sediment accumulation (after Tull, 1997).

2.1.1. Bottom simulating reflectors

Based on seismic, thermodynamic, and petrographic analysis of the BSR $TZ_{A/CT}$ accommodated within the Middle Miocene sediments of the Ocean Drilling Program (ODP) Sites 794 and 795 in the Sea of Japan, Varkouhi et al. (2020b) compiled a set of observations that indicate the opal-A to opal-CT transition zones with a BSR geometry possibly represent an actively migrating diagenetic front:

- They are found in continuous stratigraphic sections with no major breaks or unconformities in deposition;
- The front is clearly identifiable on seismic profiles;
- Though parallel to the present-day seabed, the $TZ_{A/CT}$ lies discordant to host sediments (Hein et al., 1978; Figs. 4 A through C);
- The front is hosted in silica-rich young sediments (Late Miocene and younger). The age of depositional horizons hosting the $TZ_{A/CT}$ was constrained by diatom biostratigraphy (Shipboard Scientific Party, 1990a, 1990b; Koizumi, 1992);
- The geothermal gradient of the sediment accommodating the $TZ_{A/CT}$ is very high (e.g. 132 °C/km for Site 795; Shipboard Scientific Party, 1990b)

In contrast, only a few BSR opal-A to opal-CT transitions that are parallel to the present-day seabed and are in an arrested diagenetic state have been convincingly documented. An excellent example is located in the western Pacific and was calibrated by ODP Legs 129 and 181 (Figs. 5A, B). The seismic record in the vicinity of Site 800 from Leg 129 displays a shallow deformed $TZ_{A/CT}$ reflection at a more or less constant depth of ~ 50 mbsf (equates to 0.06s two-way traveltime) that generally mimics the seabed reflector (Fig. 5A). This $TZ_{A/CT}$ lies discordant with the stratified ancient host sediments of Campanian age, but simulating the far younger (Middle Miocene to Quaternary) overlying pelagic clay beds (containing 20% opal-A in average; International Ocean Discovery Program, 2014). A large hiatus ranged from the Late Cretaceous (Early Maastrichtian) to late Early Miocene and regionally recorded over the central western Pacific has been well documented within and in proximity of this ODP borehole site (Shipboard Scientific Party, 1990c).

There are two hypotheses that account for the likely arrest of silica diagenesis across this $TZ_{A/CT}$: 1) a sudden change in thermal regime of the host basin, 2) major breaks in sediment accumulation

Since silica diagenesis is dominantly temperature controlled (Kastner et al., 1977; Kastner and Gieskes, 1983; Littke et al., 1991; Kuramoto et al., 1992; Eichhubl and Behl, 1998; Davies and Cartwright, 2002; Neagu et al., 2010b), this ancient BSR $TZ_{A/CT}$ may represent the record of a major sudden decrease in the heat flow during the arrest period, likely before the Middle Miocene, therefore accounting for its disequilibrium with the present-day geothermal gradient. If this is the case, the thin overburden that has deposited above the $TZ_{A/CT}$ since the Middle Miocene means that a Late Cretaceous to late Early Miocene hypothetical palaeo-geothermal gradient at a minimum of 70 °C/km, markedly greater than that of the present-day (the modern geothermal gradient and temperature being 50 °C/km and ~ 2.5 °C, respectively; after Shipboard Scientific Party, 1990c; Fig. 6), would have been needed to raise the palaeo-temperature of $TZ_{A/CT}$ above its modern temperature. In addition, the diagenesis was likely arrested when the $TZ_{A/CT}$ was migrating up-section through the biosiliceous overburden under a markedly higher geothermal gradient, given the discordant geometry of this transition relative to the adjacent stratigraphy. However, there are currently no constraints of the past temperature relationships to verify this hypothesis.

The Late Cretaceous to Middle Miocene phase of non-deposition coincident with the surface of the $TZ_{A/CT}$ can also lend support to the inference that the silica diagenesis across the transition zone drilled by the ODP Leg 129 is an arrested reaction front. An event of rapid reduction of overburden by deep regional marine erosion over the central western part of the Pacific Ocean (as documented by Shipboard Scientific Party, 1990c) was followed by the very low accumulation rate of post-hiatus sediments typical of pelagic deep-sea clays. This erosional event probably led to a marked decrease in the geothermal gradient such that the overburden deposited since Middle Miocene time has still not returned the arrested $TZ_{A/CT}$ level back to the temperature required to rejuvenate its active status. The fact that the $TZ_{A/CT}$ and its accommodating bedding reflectors are heavily involved in the latest phase of deformation, including faulting, while the post-hiatus Cenozoic deposits above it have not been deformed further supports this hypothesis by implying that the ancient formerly deep transition was deformed before the deposition of after-hiatus strata; thus out of thermal equilibrium, to such a degree that it cannot be still advancing up the column. In addition, development of cellular morphologies along middle parts of the transition zone (Fig. 5A) and that these features die out up-section and do not offset the opal-A-bearing beds indicate that silica diagenesis has been likely arrested before the Middle Miocene age of the initiation of post-hiatus deposits. The formation of these cellular structures across the $TZ_{A/CT}$ is attributed to the pre-arrest upward advance of this boundary due to the release of overpressure (Davies and Cartwright, 2007; Neagu et al., 2010b).

While the typical BSR $TZ_{A/CT}$ with likely arrested status are commonly observed to be 100–200 m or less of the present-day seabed, rare cases of deeper transitions (> 400 mbsf) can also be tracked through the western Pacific deep-sea sediments. The best example of this type of $TZ_{A/CT}$ was penetrated during ODP Leg 181, proximal to Site 1124 in North Island, New Zealand (Fig. 5B). This folded diagenetic horizon cross-cuts the Late Cretaceous host stratigraphy, but is parallel to the near-seabed younger strata. Over the eastern flank of the Hikurangi Trough, west of Site 1124, the $TZ_{A/CT}$ is typically parallel to the basal hemipelagic biosiliceous layers which have deposited immediately following the erosional event responsible for an Early Miocene (19–23.8 Ma) unconformity (after Shipboard Scientific Party, 1999). Although association solely with the regional folding, does not strongly support arrested diagenesis across the boundary, the initiation of diagenesis since Late Cretaceous suggests that this deeply buried ancient $TZ_{A/CT}$ cannot be related to an active diagenetic reaction in its current sub-seafloor position ~ 470 mbsf (Fig. 5B). It seems that the upward migration of the boundary was arrested in a folded geometry before the cessation of regional folding and onset of the Early Miocene erosional events. Analogous structural deformation pattern of the $TZ_{A/CT}$ and its overlying reflectors, including the current folded seabed suggests that the arrest of diagenesis pre-dated the final phase of folding; otherwise the deformed geometry of the front would have been comparatively smoothed since the Late Cretaceous onset of silica diagenesis following upward advance of the $TZ_{A/CT}$ through the overlying opal-A sediment, and this is obviously not the case for this reaction front.

— *Argument*

Since temperature is a dominant control on silica diagenesis (e.g. Neagu et al., 2010b), the active up-section migration should simulate the seafloor isotherm and isothermal reflections within shallow parts of a basin with a simple structure and homogenous sedimentation rates, i.e. a BSR $TZ_{A/CT}$ (Gretener, 1981; criterion 1 in Table 2). However, such a seabottom mimicking $TZ_{A/CT}$ geometry is very unlikely to occur in the Atlantic margin, where the thermal structure of the shallow zones of this basin has been complicated by numerous local variations in thermal regimes due to highly structured nature of the basin (by following Neagu, 2011). From this, a strong case can be made that variations in thermal structure of the basin lead to thermal disequilibrium of the $TZ_{A/CT}$ stratigraphic horizon with normal isotherms that represent modern geothermal gradients (Fig. 7). The case does not imply that present local isotherms always mirror the seabed over any structure, but a discordant-to-modern seabed reaction front is a non-isothermal marker which follows neither the seafloor nor the present isotherms (criterion 3 in Table 2). Shallow isotherms are however mainly parallel to the seabed because of the effect of cold sea water, but it depends critically on basal heat flow and thermal conductivity of the sediments (Rafferty, 2011). The disequilibrium with present-day temperature structure occurs when the front upward advancement is arrested possibly owing sudden changes in the basin thermal state (e.g. Brekke, 2000). The aforementioned case also suggests that the hypothesis of Meadows and Davies (2007)–a non-BSR reaction front may still represent an active feature, but with a sluggish upward advancement–is not correct. If correct, the geometry of the $TZ_{A/CT}$ at a regional scale would have been strongly influenced by stratigraphic array of overburden, and this is clearly not the case in the Atlantic margin and the Sea of Okhotsk. In addition, if still in thermal equilibrium with the present isotherms, i.e. an active $TZ_{A/CT}$, a reflector topologically mirroring the seabed isotherm at a regional scale would have been expected (Neagu et al., 2010b). While the discordant-to-modern seafloor $TZ_{A/CT}$ represents a partly faulted more or less smooth boundary over most part of the eastern Russia in the Sea of Okhotsk, the overburden is heavily involved in collapse features that result from sediment entrain following water flows and therefore volume loss at the level of remobilized strata (Davies et al., 2008; Fig. 3). Accordingly, the parallelism the boundary in the Sea of Okhotsk shows with the overlying strata only up to level of the Late Miocene Unconformity suggests that the $TZ_{A/CT}$ has not advanced since the Late Miocene. Following this argument, a discordant-to-modern seabed geometry can highly support the regionally arrested nature of a $TZ_{A/CT}$ at different settings.

In comparison, the reliable diagnostic criteria developed by Varkouhi et al. (2020b) in support of the view of a likely active state for the BSR $TZ_{A/CT}$ in the deep-sea sediments of the Japan Sea can be applied to analogous basins from other geographical settings. However, given the association of some BSR $TZ_{A/CT}$, e.g. those from the western Pacific margin with deformational features, additionally the old age of these reaction boundaries (Late Cretaceous), a BSR attitude relative to the present seafloor is not a definitive proof that silica diagenesis reaction across the opal-A to opal-CT transition zone is currently active.

2.2. Truncation to present seafloor

The truncation of a sub-seabottom $TZ_{A/CT}$ reflector to the present-day seabed represents regions of eroded overburden and seafloor. The overburden erosion occurs mostly due to uplift and seawater flow energy, and its intensity in the seaward vergent region is commonly greater than that of the landward vergent region (McAdoo et al., 2004). Without doubt, when uplift and/or erosion results in the cropping out of a $TZ_{A/CT}$ reflector at the present-day seabed, the only possible interpretation is that the progress of any diagenetic reactions will most likely be curtailed, and the front arrested. A good example of such a case of an outcropping diagenetic front is shown in Figure 8 from the Nankai Trough, offshore southwestern Japan. The exposure of the $TZ_{A/CT}$ at the seafloor at a high angle on the steep ridge slopes suggests a high degree of erosion, and the cessation of silica diagenesis. The exhaustion of biogenic opal stock above the transition zone due to overburden removal over the eroded ridges is the substantial cause for the arrest of the exposed $TZ_{A/CT}$ in the Nankai Trough because this process precludes silica diagenesis, and thus leads to its arrest. Varkouhi (2018) suggested that the truncation of the reaction boundary at the seafloor provides clear and independent indications of the arrest of silica diagenesis at a regional scale. Other deformation styles associated with this $TZ_{A/CT}$, including seaward dipping faults and folds further strengthen the view of its currently arrested state. The cross-cutting relationship between this faulted/folded $TZ_{A/CT}$ and its Middle to Late Pliocene host strata suggests that biogenic silica diagenesis should have commenced and continued to proceed whilst deformation occurred during the Pliocene. However, the timing of the arrest of diagenesis cannot be determined in this case, given the removal by uplift and extensive erosion of the biogenic overburden.

2.3. Regional anticlinal–synclinal morphology

The large inversion-related folds in the Faeroe-Shetland Channel, NE Atlantic margin, exhibit a clear relationship between the structural relief at the depth of the $TZ_{A/CT}$ from this basin and the nearby stratal surfaces within the accommodating sediments (after Davies and Cartwright, 2002; Fig. 7C). At a regional scale, the $TZ_{A/CT}$ is hosted in the Early to Late Miocene sediments and is itself folded with a wavelength ranging between 5 and 20 km. The fold axes mapped at the $TZ_{A/CT}$ coincide with those mapped in the over- and underlying Upper Oligocene to Late Miocene sediments, which are known to be opaline in their original depositional facies. The structural relief at the $TZ_{A/CT}$ is far less pronounced than that of its folded host strata as expected from a discordant diagenetic reflection. It is, however, concordant with the Early Pliocene Unconformity that truncates the folded strata (Fig. 7C). Using these key observations, Davies and Cartwright (2002) concluded that the $TZ_{A/CT}$ from the Faeroe-Shetland Basin likely advanced upwards during the folding, but was arrested before the cessation of folding and the last stage of erosion across the Early Pliocene Unconformity. A similar deformational relationship was observed in the adjacent Atlantic mid-Norwegian margin by Brekke (2000), who indicated that on the flanks of the large arches and domes in this area, the $TZ_{A/CT}$ reflector clearly crosscuts the domal structures, but is also observed to be itself involved in the latest phase of the arching (Fig. 9). Brekke (2000) argued that the phase transition was regionally arrested most likely in latest Miocene or Early Pliocene time. Comparable to the approach of Davies and Cartwright (2002), Neagu et al. (2010b) used the reconstruction of major fold growth history for silica diagenesis in the mid-Norwegian margin sediments to argue that the $TZ_{A/CT}$ with partial development of serrated patterns (Fig. 10A) advanced syn-folding and hosted within the Neogene deposits was arrested in situ in a folded geometry since the Late Miocene.

— *Argument*

The interpretation of Davies and Cartwright (2002) on the state of silica diagenesis in the Faeroe-Shetland basin can be argued as the $TZ_{A/CT}$ could have continued to migrate upwards after the last phase of folding, given a significant reserve of biogenic opal above this boundary for fuelling. If this is the case, the structure of the $TZ_{A/CT}$ would have been then more highly impacted by overburden architecture than by tectonic folding, and this is clearly not the geometry that the $TZ_{A/CT}$ in the Faeroe-Shetland basin currently displays. The parallelism the folded $TZ_{A/CT}$ displays relative to the Early Pliocene Unconformity surface implies that the reaction front was in thermal equilibrium with this unconformity surface before the arrest of diagenesis because the unconformity was acting as the palaeo-seabed isotherm at that time.

Possibly, following an event of uplift and rapid reduction of overburden by erosion during Early Pliocene, this palaeo-seabed became an active erosional surface which led to the cessation of silica diagenesis across the $TZ_{A/CT}$. Another piece of evidence for the arrest of silica diagenesis before the structural deformation was discontinued comes from the formation of asymmetrical toothy (serrated) features, ranging in height from 20 to 55 m, across this boundary (Fig. 10B). These sawtooth patterns form where the $TZ_{A/CT}$ commonly cross-cuts deformed strata with an inclination similar to the angle of the boundary cross-cutting them. The serrated morphology is indicative of the $TZ_{A/CT}$ preferential upward migration through opal-A rich higher stratal levels at a stair–step separation of a few tens of metres, possibly due to variations in opal-A content of overlying sediment (Meadows and Davies, 2007). These variations are most likely linked to variations across opal-A sediment bedding. Therefore, the $TZ_{A/CT}$ developed the serrated structure by advancing up through inclined opal-rich layers of the overlying interbedded succession faster than through those with lower opal-A content.

Thermodynamically, the regional folded structure of the transition zone from the research conducted by Davies and Cartwright (2002), Brekke (2000), and Neagu et al. (2010b) suggests different temperature histories experienced by its different deformed parts. This is because the reaction boundary underwent deformation (folding) concomitant with its upward advance, prior to reaching a chemical equilibrium relative to the silica diagenetic process. As a result, the internal ordering of diagenetic silica lattice is comparatively less at the anticline crest than at the syncline trough because the depression parts of the folded $TZ_{A/CT}$ clearly experience higher temperatures (Mizutani 1977; Neagu et al. 2010b). The maturation lines of cristobalite therefore do not track the present-day isothermal reflections, an indication for the cessation of ongoing diagenesis across the $TZ_{A/CT}$ (Varkouhi et al., 2020b).

2.4. Differential compaction folding

The upward migration of silica reaction boundary during the transformation of opal-A to opal-CT can result in the differential compaction and subsidence in the clastic deposits hosting silica diagenesis (Davies, 2005). The type example of this diagenetically induced folding mechanism was described from the Faeroe-Shetland Basin on the NE Atlantic margin using 3D seismic data (Davies, 2005). The folding and differential compaction was attributed to differential advance of the $TZ_{A/CT}$. This boundary developed an irregular morphology comprised of a series of ridge–depression structures across the $TZ_{A/CT}$ (Figs. 7 and 11), with a pattern of low-relief ridges or monoclines developed as areas of localized elevations spaced

~ 0.5 to ~ 1 km apart and separated by gentle depressions (Davies et al., 1999; Davies, 2005; Davies and Cartwright, 2007). The ridge–depression format has primarily developed because the host sediment mantles the polygonal fault system and the $TZ_{A/CT}$ tracks the faulted deformed stratigraphy (Davies, 2005). The accentuation of front relief through the ridge lateral/upward growth—this is possibly due to an increased local heating by the flux of hot fluids from the faults dissecting the $TZ_{A/CT}$—leads to the compaction and synchronous differential subsidence of overburden due to porosity collapse, and thereby the development of unusual domal folds, ranging in amplitude from ~ 50 m to subtle features of < 10 m, with troughs mostly aligned with the underlying frontal ridges (Fig. 11). Accordingly, the ridge–depression structure of the $TZ_{A/CT}$ has developed during onset of diagenesis, before the overburden subsiding to the depth of this boundary. Hence, the continued development of these folds implies continued upwards migration of the irregularly advancing reaction front through the overlying opal-A sediment pile. Neagu et al. (2010b) used this criterion to argue for cessation of active upward migration of the $TZ_{A/CT}$ from the mid-Norwegian margin.

— *Argument*

The structural relief of domal folds systematically decreases upwards, keeping in pace with decrease in rate of active differential advance of the $TZ_{A/CT}$ (Fig. 11; criterion 5 in Table 2). From this interpretation, Neagu et al. (2010b) made a case that by the end of differential compaction folding process, all active up-section migration of the $TZ_{A/CT}$ from the mid-Norwegian margin ceased at a regional scale, i.e. a presently arrested transition. However, the same morphology could occur if one assumes silica diagenesis commenced since Early Miocene is probably still ongoing across the $TZ_{A/CT}$, albeit for the time being at a rate that is slow enough (lower than the burial rates of the order of meters per million years; Varkouhi et al., 2021) to develop the fold relief and width comparable to those progressively formed due to earlier opal-A to opal-CT transformation. Accordingly, the systematic upward decrease in the fold relief is consistent with a significant reduction in differential porosity collapse (Fig. 11) which is essentially impacted by the rate of silica diagenetic reaction (e.g. Mizutani, 1970, 1971, 1977; Varkouhi et al., 2020a; Varkouhi et al., 2020b). As a conclusion, association with this mode of deformation cannot independently provide strong supporting evidence that the silica transition zones accommodated within the Neogene deposits of the Faeroe-Shetland basin and mid-Norwegian margin are currently arrested reaction fronts.

2.5. Polygonal faults

Polygonal fault systems are widely developed in biosiliceous mudstones that accumulate on many continental margins, abyssal plains, and some foreland basins and are linked to sediment compaction and fluid expulsion (Cartwright, 1994, 2011; Cartwright and Dewhurst, 1998; Berndt et al., 2003; Stuevold et al., 2003; Gay and Berndt, 2007; He et al., 2010; Ding et al., 2013). The individual faults making up the polygonal fault system have small throws (commonly <50 m; Figs. 7A–C), and propagate with a diverse range of strikes such that the array appears polygonal in planform (Cartwright et al., 2003; Cartwright, 2007). This polygonality of the array is the defining feature of the system as a whole, and is one of the main pieces of supportive evidence leading to the conclusion that polygonal faults are not formed as a result of regional tectonic stresses (Cartwright, 2007). Using data from 3D mapping of the NE Atlantic margin basins offshore UK and Norway, Cartwright and Dewhurst (1998) showed that the $TZ_{A/CT}$ is hosted within polygonally faulted Early to Late Miocene biosiliceous muds over most of the margin from the Rockall Basin in the southwest to the Vøring Basin in the northeast. Further research on geometry and characteristics of the polygonally faulted and deformed $TZ_{A/CT}$ along the Norwegian margin (Cartwright, 2007; Neagu, 2010b) revealed that the magnitude of the throw at the level of the $TZ_{A/CT}$ across each extensional polygonal fault is typically less than the true stratigraphic throw of the host stratigraphy on the same fault (Figs. 7A, B). This key observation has been attributed to the arrest of silica diagenesis, possibly since Late Miocene, prior to the last phase of faulting across the $TZ_{A/CT}$ and its nearby strata (Cartwright, 2007; Neagu et al., 2010a; Neagu et al., 2010b).

— *Argument*

Having accumulated the minimum local throw values at the level of the $TZ_{A/CT}$ in the mid-Norwegian margin, while a substantial proportion of the total fault displacement actively accumulated on the fault surface above and below the position of the $TZ_{A/CT}$ may reveal the activity of a post-arrest phase of fault growth (Neagu et al., 2010a). Furthermore, the upper fault tip displacement distribution argues that the post-arrest youngest active fault phase results in the shallowest tip propagation and these faults have the largest offsets of the $TZ_{A/CT}$ (Neagu et al., 2010a). The usually greater throw in the opal-CT interval below the $TZ_{A/CT}$ and the effective cessation of displacement in the interval above it seem consistent with the suggested notion of an arrested upward migration of silica diagenesis within the deep-sea sediments of NE Atlantic margin. This scenario is however plausible only if the displacement rate of the fault was equal to or less than the ascent rate of the migrating diagenetic front prior to the arrest of diagenesis and the last period of faulting (Fig. 12). Contrary to this scenario, the same relationship (the $TZ_{A/CT}$ throw across polygonal faults lower than the true stratigraphic offset) could occur during active silica diagenesis if the fault displacement rate was higher than the rate of $TZ_{A/CT}$ migration through the overlying opal-A sediment in the NE Atlantic margin basins. This interpretation accords with findings of Shin et al. (2008), Cartwright (2011), Davies and Ireland (2011), and Hooker et al. (2017) concerning syn-diagenetic origin of polygonal faults. According to these works, particle dissolution during diagenesis may cause contraction of host stratigraphy, sediment failure, and hence polygonal faulting. Marked displacement accumulation on the faults above and below the $TZ_{A/CT}$, compared to the displacement minima at the depth of this boundary, can be related to strain softening of the host strata during ongoing diagenesis, which leads to the later failure along existing faults (after Wrona et al., 2017b). Due to their massively different material behaviour, the shear strength of opal-CT cemented mudstones is however higher than that of opal-A uncemented sediments (Bjorlykke and Hoeg, 1997), therefore the strain softening of cemented mudstones would need to be experimentally validated. Furthermore, the second scenario (fault displacement rates higher than the rate of $TZ_{A/CT}$ upward advance) is possible if very low rates of the order of mm per 1000 years for $TZ_{A/CT}$ migration are assumed, but these rates are effectively static relative to the burial and heating rate. Following these opposite scenarios, the evidence offered based solely on polygonal faults is not strong proof of the present-day diagenetic state of the $TZ_{A/CT}$, i.e. whether silica diagenesis across the opal-A to opal-CT transition zone is an arrested reaction.

3. Discussion

From the preceding review of criteria for determining the diagenetic state of silica reaction boundaries, it is evident that relationships between the $TZ_{A/CT}$ and contemporaneous deformation, including polygonal faults, differential compaction folds, and tectonic folds can provide firm indications of the arrest of the upward migration of a silica diagenetic front at a regional scale (Neagu et al., 2010b; Table 2) . Individual examples of each mode of deformation and their relationship to the $TZ_{A/CT}$ is not as convincing for assessing the putative arrest of the $TZ_{A/CT}$ as when disparate lines of evidence point in the same direction. In case of the mid-Norwegian margin section, for instance, as documented by Neagu et al. (2010b), the obviously smaller offset of the $TZ_{A/CT}$ at each polygonal fault than the true offset of embedding strata could comparably occur either concomitant with upward ascent of the boundary or after the cessation of silica diagenesis, as for the $TZ_{A/CT}$ from the NE Atlantic basin offshore UK (Davies and Cartwright, 2002). Observation of the systematic attenuation of differential folding process through the shallower strata overlying the transition zone either proportional to the sluggish upward advance of the $TZ_{A/CT}$ or prior to arrest of silica diagenesis suggests that a line of evidence based only on differential compaction folding is not a solid record for arrest of silica diagenesis across the $TZ_{A/CT}$ in these basins. Regional folding of the $TZ_{A/CT}$ offers to some extent more reliable arrest proofs of silica diagenesis than the polygonal faults and differential compaction folds, provided that in both basins the deformed geometry of the $TZ_{A/CT}$ has been commonly more impacted and complicated by anticlinal–synclinal systems than overburden architecture.

Compared to the deformational patterns discussed, discordance relative to present-day thermal structure and possible exposure at seafloor are more credible diagnostic criteria for arbitrating the diagenetic state of a $TZ_{A/CT}$ at a regional scale. The non-parallel geometry of a $TZ_{A/CT}$ with the seabed and present-day isotherms provides strong record of regional arrest as documented by Roaldset and He (1995) for the $TZ_{A/CT}$ from the Barents Sea sediments and by Brekke (2000) and Neagu et al. (2010b) for the $TZ_{A/CT}$ in the mid-Norwegian margin, given that local heat flow anomalies have caused the thermal structure of these basins to become intricate, and have thus led to marked deviations of the $TZ_{A/CT}$ from correspondence to present isotherms. Due to heat flow variations in the host basin, the $TZ_{A/CT}$ has departed from equilibrium with temperature field in the basin; thus the non-parallelism of this boundary with isothermal reflections. The contradictory interpretation for current state of the regionally discordant-to-seabed $TZ_{A/CT}$ from the Sea of Okhotsk proposed by Meadows and Davies (2007) was challenged here, given that the reaction boundary has been more highly complicated by structural deformations than by the geometry of its overburden. In contrast, a BSR attitude can equally represent either active or arrested status of a $TZ_{A/CT}$ as indicated by Varkouhi et al. (2020) for the likely active characteristic of the transition zone penetrated by the ODP Wells 794 and 795, but the arrested nature of the BSR $TZ_{A/CT}$ drilled by the ODP Site 800. From this, a case can be made that while a non-BSR feature strongly supports arrested state of a $TZ_{A/CT}$, a BSR geometry is not an independent reliable proof of ongoing silica diagenesis. Among the seismic/structural criteria so far offered for diagenetic diagnosis of the state of a $TZ_{A/CT}$, its truncation to the seabed as suggested by Varkouhi (2018) is the only process that independently and with certainty leads to the arrest of diagenesis, provided that overburden reduction and seafloor exposure of the $TZ_{A/CT}$ cause running out of opal reserve of the sediment, which results in the cessation of biogenic silica diagenetic reaction. In case of the $TZ_{A/CT}$ tracked in the deep-sea sediments from offshore southwestern Japan, the discordant attitude this deformed (faulted/folded) and truncated boundary takes relative to the seabed and the strata just below it indicates thermal disequilibrium of silica diagenesis reaction with present temperature–depth relationships, and hence with the present-day isotherms in this region.

In conclusion, to draw a reliable interpretation for silica diagenesis in depositional settings at a regional scale using seismic data, the recognition criteria reviewed above should all together be taken into account in each study case. In case of the Nankai Trough $TZ_{A/CT}$, for example, even though the exposure at the seabed is a certain indication for the arrest of its upward advance, association with other modes of deformation, such as faulting and folding have been utilised to further construe the arrested status of this reaction front. These interpretational criteria of contribution the seismic/structural approach makes to the understanding of silica diagenetic process are so far used by a small spectrum of research over the past decades. This is, to the authors' knowledge, because seismic stratigraphy is yet in its infancy stage and major advances in this research tool came first in the early 1980s with the advent of 3D seismic mapping, and that high-resolution surveying this method offers has only recently stimulated a new approach to the study of silica diagenesis. Because of its limited vertical resolution, the seismic stratigraphy contains some fallibility, however the usage of this medium still remains the most reliable method for the study of silica diagenesis at a basin scale.

Acknowledgments

Dr. Thilo Wrona, Helmholtz Centre Potsdam – GFZ German Research Centre for Geosciences, and Dr. John N. Hooker, University of the Incarnate Word, are thanked for their constructive and thorough reviews. Dr. Peter M. Burgess, an associate editor of Basin Research, is thanked for his considered independent review of this paper. Permission to include seismic profiles is warmly acknowledged from International Ocean Discovery Program (IODP), ODP, and Statoil. R.C. Neagu is thanked for permission to include Figure 2, R.J. Davies for Figures 3 and 7C, J.A. Cartwright for Figure 7A, B.G. McAdoo for Figure 8, and P. Blystad for Figure 9. The authors declare no conflicts of interest.

References

Behl, R.J., and Garrison, R.E. 1994. The origin of chert in the Monterey Formation of California (USA). *In* Iijima, A., Abed, A., Garrison, R. (Eds.), Siliceous, Phosphatic and Glauconitic Sediments of the Tertiary and Mesozoic, Proceedings of the 29th International Geological Congress, Part C, Utrecht, The Netherlands, p. 101–132.

Berndt, C., Bünz, S., and Mienert, J. 2003. Polygonal fault systems on the mid-Norwegian margin: A long-term source for fluid flow, *Geological Society of London Special Publications*, 216, p. 283–290.

Bjorlykke, K., and Hoeg, K. 1997. Effects of burial diagenesis on stresses, compaction and fluid flow in sedimentary basins, *Marine and Petroleum Geology*, 14, 267–276.

Blystad, P., Brekke, H., Færseth, R.B., Larsen, B.T., Skogseid, J., and Tørudbakken, B. 1995. Structural elements of the Norwegian Continental Shelf. Part II: The Norwegian Sea Region, *Norwegian Petroleum Directorate Bulletin*, No. 8.

Brekke, H. 2000. The Tectonic Evolution of the Norwegian Sea Continental Margin with Emphasis on the Vøring and Møre Basins, *Geological Society of London Special Publications*, 167, p. 327–378.

Cartwright, J.A. 1994. Episodic basin-wide hydrofracturing of overpressured Early Cenozoic mudrock sequences in the North Sea Basin, *Marine and Petroleum Geology*, 11, p. 587–607.

Cartwright, J.A. 2007. The impact of 3D seismic data on the understanding of compaction, fluid flow and diagenesis in sedimentary basins, *Journal of the Geological Society*, 164, p. 881–893.

Cartwright, J.A. 2011. Diagenetically induced shear failure of fine-grained sediments and the development of polygonal fault systems, *Marine and Petroleum Geology*, 28, p. 1593–1610.

Cartwright, J.A., and Dewhurst, D. 1998. Layer-bound compaction faults in finegrained sediments, *Geological Society of America Bulletin*, 110, p. 1242–1257.

Cartwright, J., James, D., and Bolton, A. 2003. The genesis of polygonal fault systems: A review, *Geological Society of London Special Publications*, 216, p. 223–243.

Chaika, C. 1998. Physical Properties and Silica Diagenesis, PhD thesis, Stanford University, 130 p.

Chaika, C., and Dvorkin, J. 1997. Ultrasonic velocities of opaline rocks undergoing silica diagenesis, *Geophysical Research Letters*, 24, p. 2039–2042.

Chaika, C., and Dvorkin, J. 2000. Porosity reduction during diagenesis of diatomaceous rocks, *American Association of Petroleum Geologists Bulletin*, 84, p. 1173–1184.

Chaika, C., and Williams, L.A. 2001. Density and mineralogy variations as a function of porosity in Miocene Monterey Formation oil and gas reservoirs in California, *American Association of Petroleum Geologists Bulletin*, 85, p. 149–167.

Davies, R.J. 2005. Differential compaction and subsidence in sedimentary basins due to silica diagenesis: A case study, *Geological Society of America Bulletin*, 117, p. 1146–1155.

Davies, R.J., and Cartwright, J. 2002. A fossilized Opal A to Opal C/T transformation on the northeast Atlantic margin: Support for a significantly elevated palaeogeothermal gradient during the Neogene?, *Basin Research*, 14, p. 467–486.

Davies, R.J., and Cartwright, J.A. 2007. Kilometer-scale chemical reaction boundary patterns and deformation in sedimentary rocks, *Earth and Planetary Science Letters*, 262, p. 125–137.

Davies, R.J., and Ireland, M.T. 2011. Initiation and propagation of polygonal fault arrays by thermally triggered volume reduction reactions in siliceous sediment, *Marine Geology*, 289, p. 150–158.

Davies, R.J., Cartwright, J.A., and Rana, J. 1999. Giant hummocks in deep-water marine sediments: Evidence for large-scale differential compaction and density inversion during early burial, *Geology*, 27, p. 907–910.

Davies, R.J., Goulty, N.R., and Meadows, D. 2008. Fluid flow due to the advance of basin-scale silica reaction zones, *Geological Society of America Bulletin*, 120, p. 195–206.

Davies, R.J., Ireland, M.T., and Cartwright, J.A. 2009. Differential compaction due to the irregular topology of a diagenetic reaction boundary: A new mechanism for the formation of polygonal faults, *Basin Research*, 21, p. 354–359.

Dillon, W.P., Lee, M.W., Fehlhaber, K. and Coleman, D.F. 1993. Gas hydrates on the Atlantic margin of the United States - controls on concentration. *In* Howell, D.G. (Ed.), The Future of Energy Gases, *U.S. Geological Survey Professional Paper 1570*, p. 313–330.

Ding, X., Liu, G., Sun, M., and Wang, P. 2013. Origin of polygonal fault systems: A case from the Sanzhao sag in the Songliao Basin, East China, *Petroleum Exploration and Development*, 40, p. 333–343.

Dralus, D. , Lewan, M.D. , and Peters, K. 2015. Kinetics of the opal-A to opal-CT phase transition in low- and high-TOC siliceous shale source rocks, American Association of Petroleum Geologists Annual Convention & Exhibition, Denver, Colorado.

Eichhubl, P., and Behl, R.J. 1998. Diagenesis, deformation, and fluid flow in the Miocene Monterey Formation of coastal California. *In* Eichhubl. P., (Ed.), Diagenesis, deformation, and fluid flow in the Miocene Monterey Formation of coastal California, *SEPM Pacific Section Special Publication*, 83, p. 5–13.

Emerson, S.R., and Hedges, J.I. 2008. Chemical Oceanography and the Marine Carbon Cycle, Cambridge, Cambridge University Press, 453 p.

Gay, A., and Berndt, C. 2007. Cessation/reactivation of polygonal faulting and effects on fluid flow in the Vøring Basin, Norwegian Margin, *Journal of the Geological Society*, 164, p. 129–141.

Gretener, P.E. 1981. Geothermics: Using temperature for hydrocarbon exploration. *In* Education Course Note Series #17, American Association of Petroleum Geologists, Tulsa, Oklahoma, USA, 170 p.

He, C., Tang, L., Huang, D., and Shi, S. 2010. Polygonal faults in the Sanzhao sag of the Songliao basin: Their significance in hydrocarbon accumulation, *Mining Science and Technology*, 20, p. 300–305.

Hein, J.R., Scholl, D.W., Barron, J.A., Jones, M.G., and Miller, J. 1978. Diagenesis of late Cenozoic diatomaceous deposits and formation of the bottom simulating reflector in the southern Bering Sea, *Sedimentology*, 25, p. 155–181.

Hillman, J.I.T., Cook, A.E., Sawyer, D.E., Küçük, H.M., Goldberg, D.S. 2017. The character and amplitude of ‘discontinuous’ bottom-simulating reflections in marine seismic data, *Earth and Planetary Science Letters,* 459, p. 157–169.

Hooker, J.N., Huggett, J.M., Cartwright, J., and Ali Hussein, M. 2017. Regional-scale development of opening-mode calcite veins due to silica diagenesis. G3*, Geochemistry, Geophysics, Geosystems*, 18, p. 2580–2600.

International Ocean Discovery Program. 2014. Retrieved from http://web.iodp.tamu.edu/OVERVIEW/

International Ocean Discovery Program Site Survey Data Bank. 2019. Retrieved from https://ssdb.iodp.org/SSDBquery/SSDBlegacy.php?xml=legacy_d.xml

Ireland, M.T., Goulty, N.R., and Davies, R.J. 2010. Influence of pore water chemistry on silica diagenesis: evidence from the interaction of diagenetic reaction zones with polygonal fault systems, *Journal of the Geological Society*, 167, p. 273–279.

Isaacs, C.M. 1981. Porosity reduction during diagenesis of the Monterey Formation, Santa Barbara coastal area, California. *In* Garrison, R.E., and Douglas, R.G. (Eds.), The Monterey Formation and Related Siliceous Rocks of California: Pacific Section, Society of Economic Paleontologists and Mineralogists Special Publication, 15, p. 257–272.

Isaacs, C.M. 1982. Influence of rock composition on kinetics of silica phase changes in the Monterey formation, Santa Barbara area, California, *Geology*, 10, p. 304–308.

Kastner, M., and Gieskes, J.M. 1983. Opal-A to opal-CT transformation: A kinetic study. *In* Iijima, A., Hein, J.R., and Siever, R., (Eds.), Siliceous Deposits in the Pacific Region: Amsterdam, Elsevier Science Publishing Company, p. 211–227.

Kastner, M., Keene, J.B., and Gieskes, J.M. 1977. Diagenesis of siliceous oozes — I. Chemical controls on the rate of opal-A to opal-CT transformation — an experimental study, *Geochimica et Cosmochimica Acta*, 41, p. 1041–1059.

Keller, M.A., and Isaacs, C.M. 1985. An Evaluation of Temperature Scales for Silica Diagenesis in Diatomaceous Sequences Including a New Approach Based on the Miocene Monterey Formation, California, *Geo-Marine Letters*, 5, p. 31–35.

Koizumi, I. 1992. Diatom biostratigraphy of the Japan Sea: Leg 127. *In* Pisciotto, K.A., Ingle, J.C., Jr., von Breymann, M.T., Barron, J., et al., (Eds.), Proceedings of the Ocean Drilling Program, Scientific Results, College Station, Texas, 127/128 (Pt. 1), p. 249–289.

Kuramoto, S., Tamaki, K., Langseth, M.G., Nobes, D.C., Tokuyama, H., Pisciotto, K.A., and Taira, A. 1992. Can opal-A/opal-CT BSR be an indicator of the thermal structure of the Yamato Basin, Japan Sea?. *In* Tamaki, K., Suyehiro, K., Allan, J., McWilliams, M., et al., (Eds.), Proceedings of the Ocean Drilling Program, Scientific Results, College Station, Texas , 127/128, p. 1145–1156.

Leeder, M.R. 1982. Sedimentology: Process and Product, Allen and Unwin, London, 344 p.

Littke, R., Fourtanier, E., Thurow, J., and Taylor, E. 1991. Silica diagenesis and its effects on lithification of Broken Ridge deposits, Central Indian Ocean. *In* Peirce, J., Weissel, J., et al. (Eds.), Proceedings of the Ocean Drilling Program, Scientific Results, College Station, Texas, 121, p. 261–272.

Lonsdale, M.J. 1990. The relationship between silica diagenesis, methane, and seismic reflections on the South Orkney microcontinent. *In* Barker, P.F., Kennet J.P., et al. (Eds.), Proceedings of the Ocean Drilling Program, Scientific Results, College Station, Texas, 113, p. 27–37.

Loucaides, S., Michalopoulos, P., Presti, M., Koning, E., Behrends, T., and Van Cappellen, P. 2010. Seawater-mediated interactions between diatomaceous silica and terrigenous sediments: Results from long-term incubation experiments, *Chemical Geology*, 270, p. 68–79.

Lyle, M., Gallaway, P.J., Liberty, L.M., Mix, A., Stott, L., Hammond, D., Gardner, J., Dean, W., and the EW9504 Scientific Party. 1995a. Data submission. W9406 and EW9504 site surveys of the California margin proposed drilling sites, Leg 167 (v. 1): Site maps and descriptions, CGISS Technical Reports 95-11, Boise State University, 167 p.

Lyle, M., Gallaway, P.J., Liberty, L.M., Mix, A., Stott, L., Hammond, D., Gardner, J., Dean, W., and the EW9504 Scientific Party. 1995b. Data submission. W9406 and EW9504 site surveys of the California margin proposed drilling sites, Leg 167 (v. 2): Seismic profiles, CGISS Technical Reports 95-12, Boise State University, 242 p.

McAdoo, B.G., Capone, M.K., and Minder, J. 2004. Seafloor geomorphology of convergent margins: Implications for Cascadia seismic hazard, *Tectonics*, 23, TC6008.

Meadows, D., and Davies, R.J. 2007. Morphological development of basin-scale silica diagenetic fronts revealed with 2D seismic reflection data: offshore Sakhalin, Russian Far East, *Journal of the Geological Society*, 164, p. 1193–1206.

Meadows, D. and Davies, R.J. 2009. Predicting porosity reduction due to silica diagenesis using seismic reflection data, *Marine and Petroleum Geology*, 26, p. 1543–1553.

Mizutani, S. 1970. Silica minerals in the early stage of diagenesis, *Sedimentology*, 15, p. 419–436.

Mizutani, S. 1971. Silica minerals in diagenesis, Memoir 6. Geological Society of Japan, p. 151–163 (in Japanese).

Mizutani, S. 1977. Progressive ordering of cristobalitic silica in the early stage of diagenesis, *Contributions to Mineralogy and Petrology*, 61, p. 129–140.

Neagu, R.C. 2011. The relationship between biogenic silica diagenesis and the physical properties of sediments studied using seismic and well data, PhD thesis, Cardiff University, 275 p.

Neagu, R.C., Cartwright, J., and Davies, R. 2010a. Measurement of diagenetic compaction strain from quantitative analysis of fault plane dip, *Journal of Structural Geology*, 32, p. 641–655.

Neagu, R.C., Cartwright, J., Davies, R.J., and Jensen, L. 2010b. Fossilisation of a silica diagenesis reaction front on the mid-Norwegian margin, *Marine and Petroleum Geology*, 27, p. 2141–2155.

Nobes, D.C., Murray, R.W., Kuramoto, S., Pisciotto, K.A., and Holler, P. 1992. Impact of silica diagenesis on physical property variations. *In* Pisciotto, K.A., Ingle, J.C., Jr., von Breymann, M.T., Barron, J., et al. (Eds.), Proceedings of the Ocean Drilling Program, Scientific Results, College Station, Texas, 127/128 (Pt. 1), p. 3–31.

Ocean Drilling Program Publication Services. 2012. Retrieved from http://www-odp.tamu.edu/publications/

Ohde, A., Otsuka, H., Kioka, A., and Ashi, J. 2018. Distribution and depth of bottom-simulating reflectors in the Nankai subduction margin, *Earth Planets Space*, 70, https://doi.org/10.1186/s40623-018-0833-5

Perrodon, A., Laherrère, J.H., and Campbell, C.J. 1998. The world's non-conventional oil and gas, *Petroleum Economist*, 113 p.

Pisciotto, K.A. 1981. Diagenetic trends in the siliceous facies of the Monterey Shale in the Santa Maria region, California, *Sedimentology*, 28, p. 547–571.

Pisciotto, K.A., Murray, R.W., and Brumsack, H.J. 1992. Thermal history of Japan Sea sediments from isotopic studies of diagenetic silica and associated pore waters. *In* Pisciotto, K.A., Ingle, J.C., Jr., von Breymann, M.T., Barron, J., et al. (Eds.), Proceedings of the Ocean Drilling Program, Scientific Results, College Station, Texas, 127/128 (Pt. 1), p. 49–56.

Rafferty, J.P. 2011. Oceans and Oceanography (The Living Earth), Rosen Education Service, 266 p.

Roaldset, E., and He, W. 1995. Silica-phase transformation of opal-A to opal-CT to quartz–An experimental approach, Report, Department of Geology and Mineral Resources Engineering, Norwegian Institute of Technology, Trondheim.

Roberts, D.T. 2014. A geomechanical analysis of the formation and evolution of Polygonal Fault Systems, PhD thesis, Cardiff University, 271 p.

Sheriff, R.E., and Geldart, L.P. 1995. Exploration Seismology (2nd Ed.), New York: Cambridge University Press, 592 p.

Shin, H., Santarnarina, J.C., and Cartwright, J.A. 2008. Contraction-driven shear failure in compacting uncemented sediments, *Geology*, 36, p. 931–934.

Shipboard Scientific Party. 1990a. Site 794. *In* Tamaki, K., Pisciotto, K., Allan, J., et al., (Eds.), Proceedings of the Ocean Drilling Program, Initial Reports, College Station, Texas, 127, p. 71–167.

Shipboard Scientific Party. 1990b. Site 795. *In* Tamaki, K., Pisciotto, K., Allan, J., et al., (Eds.), Proceedings of the Ocean Drilling Program, Initial Reports, College Station, Texas, 127, p. 169–245.

Shipboard Scientific Party. 1990c. Site 800. *In* Lancelot, Y., Larson, R.L., et al., (Eds.), Proceedings of the Ocean Drilling Program, Initial Reports, College Station, Texas, 129, p. 33–89.

Shipboard Scientific Party. 1997. Site 1022. *In* Lyle, M., Koizumi, I., Richter, C., et al., (Eds.), Proceedings of the Ocean Drilling Program, Initial Reports, College Station, Texas, v. 167, p. 461–495.

Shipboard Scientific Party. 1999. Site 1124: Rekohu Drift—From the K/T boundary to the deep western boundary current. *In* Carter, R.M., McCave, I.N., Richter, C., Carter, L., et al., (Eds.), Proceedings of the Ocean Drilling Program, Initial Reports, College Station, Texas, 181, p. 1–137.

Stein, C.L., and Kirkpatrick, R.J. 1976. Experimental porcelanite recrystallization kinetics: A nucleation and growth model, *Journal of Sedimentary Petrology*, 46, p. 430–435.

Stuevold, L.M., Faerseth, R.B., Amesen, L., Cartwright, J., and Moller, N. 2003. Polygonal faults in the Ormen Lange Field, More Basin, offshore Mid Norway, *Geological Society Special Publications* 216, 263–281.

Tada, R. 1991. Compaction and cementation in siliceous rocks and their possible effect on bedding enhancement. *In* Einsele, G., Ricken, W., and Seilacher, A. (Eds.), Cycles and Events in Stratigraphy: Berlin, Springer-Verlag, p. 480–491.

Tull, S.J. 1997. The diversity of hydrocarbon habitat in Russia, *Petroleum Geoscience*, 3, p. 315–325.

Varkouhi, S. 2018. Biogenic silica diagenesis under early burial in hemipelagic marine sediments, D.Phil. thesis, University of Oxford, 428 p.

Varkouhi, S., and Wells, J. 2020. The relation between temperature and silica benthic exchange rates and implications for near-seabed formation of diagenetic opal, *Results in Geophysical Sciences*, 1–4, 100002.

Varkouhi, S., Cartwright, J.A., and Tosca, N.J. 2020a. Anomalous compaction due to silica diagenesis — Textural and mineralogical evidence from hemipelagic deep-sea sediments, *Marine Geology*, 426, p. 106204.

Varkouhi, S., Tosca, N.J., and Cartwright, J.A. 2020b. Pore water chemistry — A proxy for tracking the signature of ongoing silica diagenesis, *Journal of Sedimentary Research*, 90, p. 1037–1067.

Varkouhi, S., Tosca, N.J., and Cartwright, J.A. 2021. Temperature–time relationships and their implications for thermal history and modelling of silica diagenesis in deep-sea sediments, *Marine Geology*, 439, 106541.

Weller, R., and Behl, R.J. 2015. Physical and mechanical characteristics of the opal-A to opal-CT transition zone: Enhanced diatomite permeability from heterogeneous diagenetic embrittlement: Oxnard, California, Pacific Section of American Association of Petroleum Geologists, Society of Economic Geologists, and Society for Sedimentary Geology, Joint Technical Conference.

Williams, L.A., Parks, G.A., and Crerar, D.A. 1985. Silica diagenesis, I. Solubility controls, *Journal of Sedimentary Petrology*, 55, p. 301–311.

Williams, L.A., and Crerar, D.A. 1985. Silica diagenesis, II. General mechanisms, *Journal of Sedimentary Petrology*, 55, p. 312–321.

Wrona, T., Jackson, C.A.-L., Huuse, M., and Taylor, K.G. 2017a. Silica diagenesis in Cenozoic mudstones of the North Viking Graben: physical properties and basin modelling, *Basin Research*, 29, p. 556–575.

Wrona, T., Magee, C., Jackson, C.A.-L., Huuse, M., and Taylor, K.G. 2017b. Kinematics of polygonal fault systems: Observations from the Northern North Sea, *Frontiers in Earth Science*, 5, 101.

Wrona, T., Taylor, K.G., Jackson, C. A.-L., Huuse, M., Najorka, J., and Pan, I. 2017c. Impact of silica diagenesis on the porosity of fine-grained strata: An analysis of Cenozoic mudstones from the North Sea, *Geochemistry, Geophysics, Geosystems*, 18, p. 1537–1549.

Table 1. Seismic structural criteria for recognition of arrested and likely active silica fronts.

Criteria – Arrested silica transition zones
- A non bottom simulating reflector *(Roaldset and He, 1995; Brekke, 2000; Neagu et al., 2010b)*
- Exposure at present-day seafloor *(Varkouhi, 2018)*
- Taking anticlinal–synclinal geometry at a regional scale *(Brekke, 2000; Davies and Cartwright, 2002; Neagu et al., 2010b)*
- Deformation as differential compaction folding *(Neagu et al., 2010b)*
- Deformation by polygonal fault systems *(Cartwright, 2007; Neagu et al., 2010a; Neagu et al., 2010b)*
Criteria – Likely active silica transition zones
- A bottom simulating reflector *(Hein et al., 1978; Lonsdale, 1990; Neagu et al., 2010b; Varkouhi et al., 2020b)*

Table 2. A summary of the reviewed criteria for inferring the diagenetic state of $TZ_{A/CT}$, stratigraphic and thermal features/parameters related to this assessment, qualitative level of reliability for each diagnostic indicator, and the sketches for different types of geometries reviewed.

Reviewed identification criterion		Likely diagenetic status	Other determinative stratigraphic/structural and geothermal traits	Level of confidence	Schematic geometry
Number	Description				
1	Bottom simulating reflector	Active	- Age constraints of diagenetic front - Stratigraphic continuity of overlying sediment pile - Biogenic-opal content of overburden - Present-day geothermal gradient of host sediment	Moderately reliable	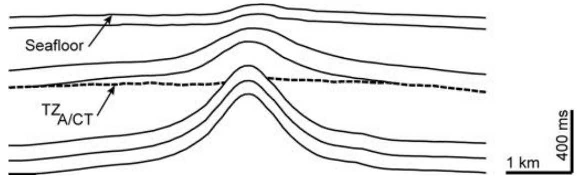
2	Exposure at present seafloor	Arrested	- Discordance relative to near-seabed stratigraphy - Response to tectonic deformation of host strata - Biogenic-silica reserve of overburden	Definitely reliable	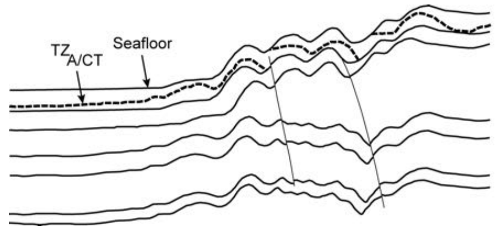
3	Non bottom simulating reflector	Arrested	- Thermal disequilibrium with modern isotherms - Structure more impacted by deformation than by overburden architecture - Age constraints of diagenetic front	Highly reliable	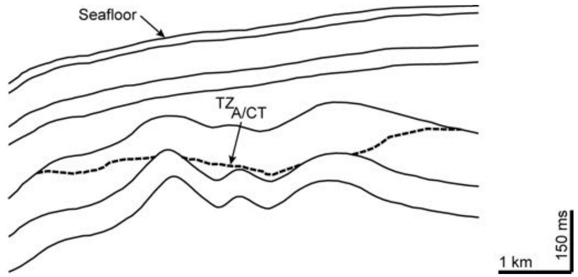

Table 2. Continued.

4	Regional anticlinal–synclinal morphology	Arrested	- Thermal-history contrast among different deformed parts of diagenetic front - Geometric pattern more influenced by structural deformation than by stratigraphic array of overburden	Moderately reliable	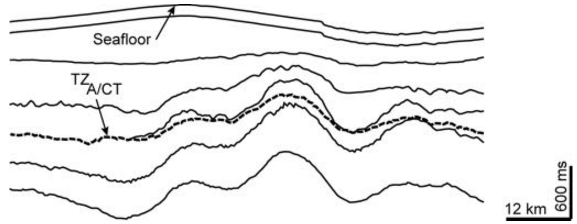
5	Differential compaction folding	Arrested	- Development of cellular morphology - Petrophysical variations of host sediment - Overburden response to differential subsidence	Slightly reliable	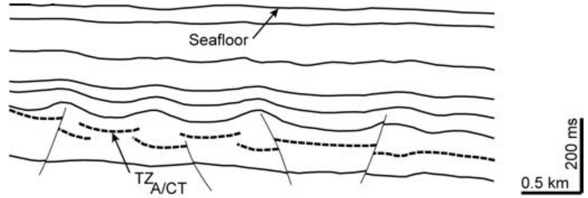
6	Polygonal faulting	Arrested	- Fault displacement contrast between diagenetic front and host stratigraphy - Non-tectonic compaction of host sediment	Slightly reliable	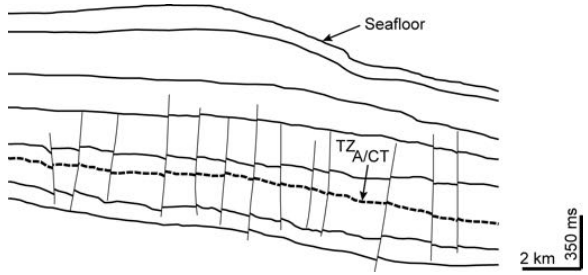
3–6	Association with various deformational styles	Arrested	- Disequilibrium with present isotherms - Marked temperature contrast across deformed zones of diagenetic front - Structure more impacted by deformation than by overburden geometry - Response to tectonic and non-tectonic compaction of host sediment and overburden - Petrophysical variability of host sediment - Age constraints of diagenetic front	Highly reliable	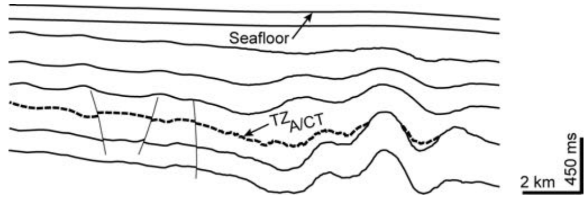

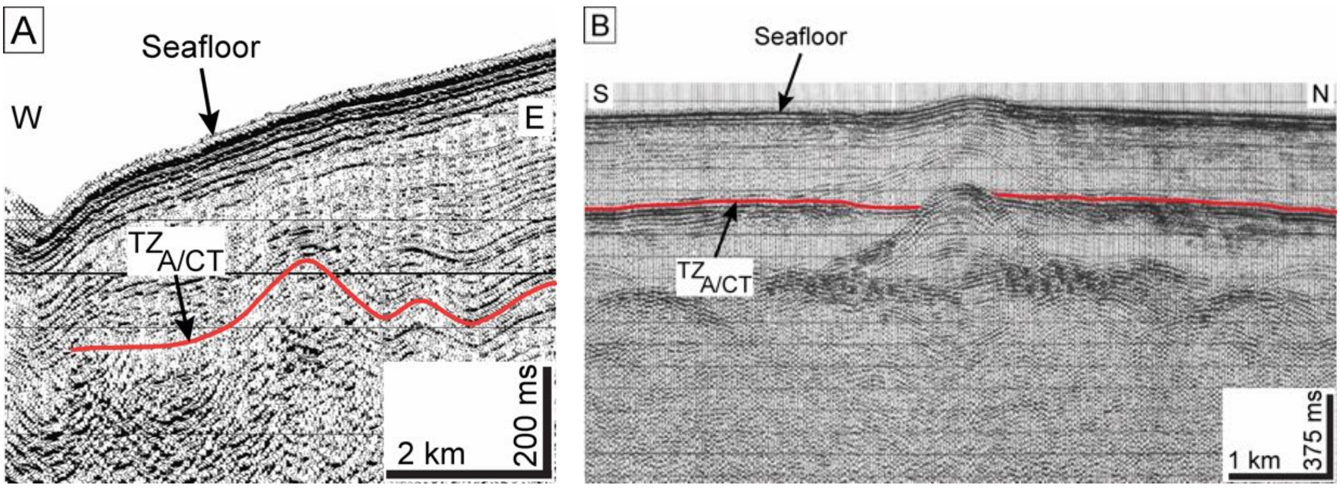

Figure 1. A regionally folded non-BSR silica diagenesis reaction front (A) versus a BSR transition zone (B). The non-BSR $TZ_{A/CT}$ captured on seismic reflection profile near the ODP Site 1022 in the California Margin represents a currently arrested boundary (modified from Lyle et al., 1995a, 1995b; Shipboard Scientific Party, 1997). The parallelism the undeformed $TZ_{A/CT}$, found on seismic section in Japan Basin, displays with the seafloor likely indicates an active boundary (modified from Shipboard Scientific Party, 1990b; Varkouhi et al., 2020b).

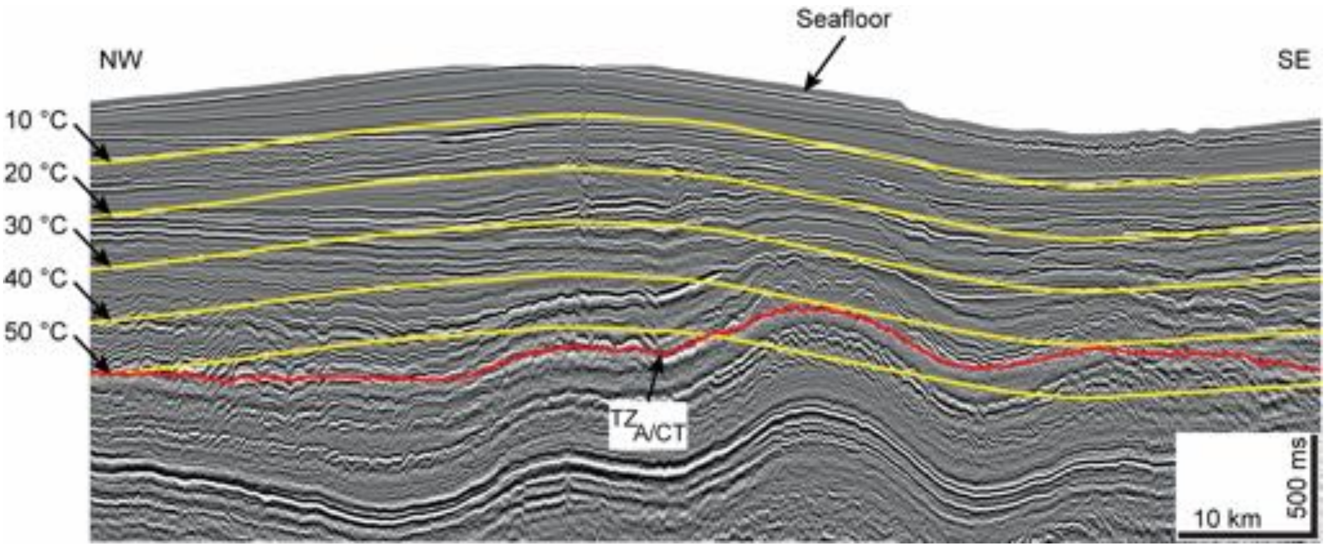

Figure 2: Seismic profile from Møre Basin, Norwegian Sea Continental Margin (modified from Neagu et al., 2010b). The regionally folded $TZ_{A/CT}$ cross-cuts the present-day isotherms (yellow lines). The isothermal curves are drawn based on the data presented in Appendix I. For simplification, an average velocity of 2000 m/s was used for the conversion of the depth of isotherms (reported in Appendix I) to the two-way travel time on this seismic section.

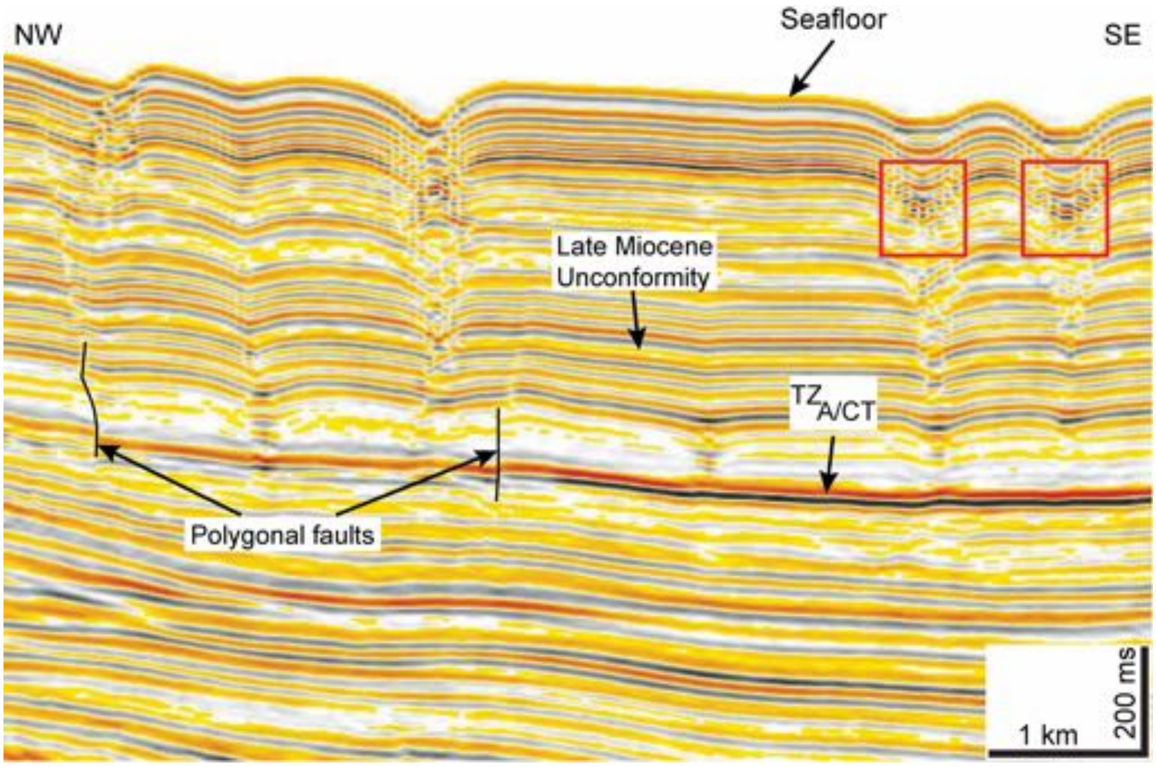

Figure 3: Two-dimensional seismic profile from offshore Sakhalin, Sea of Okhotsk showing the partly deformed $TZ_{A/CT}$ (by polygonal faults) mimicking the Late Miocene Unconformity above it (modified from Davies et al., 2008). Refer to Section 2.5 for a review of polygonal faults. Note the development of funnel-shaped collapse features (red rectangles) as fluid-scape structures above the level of the unconformity.

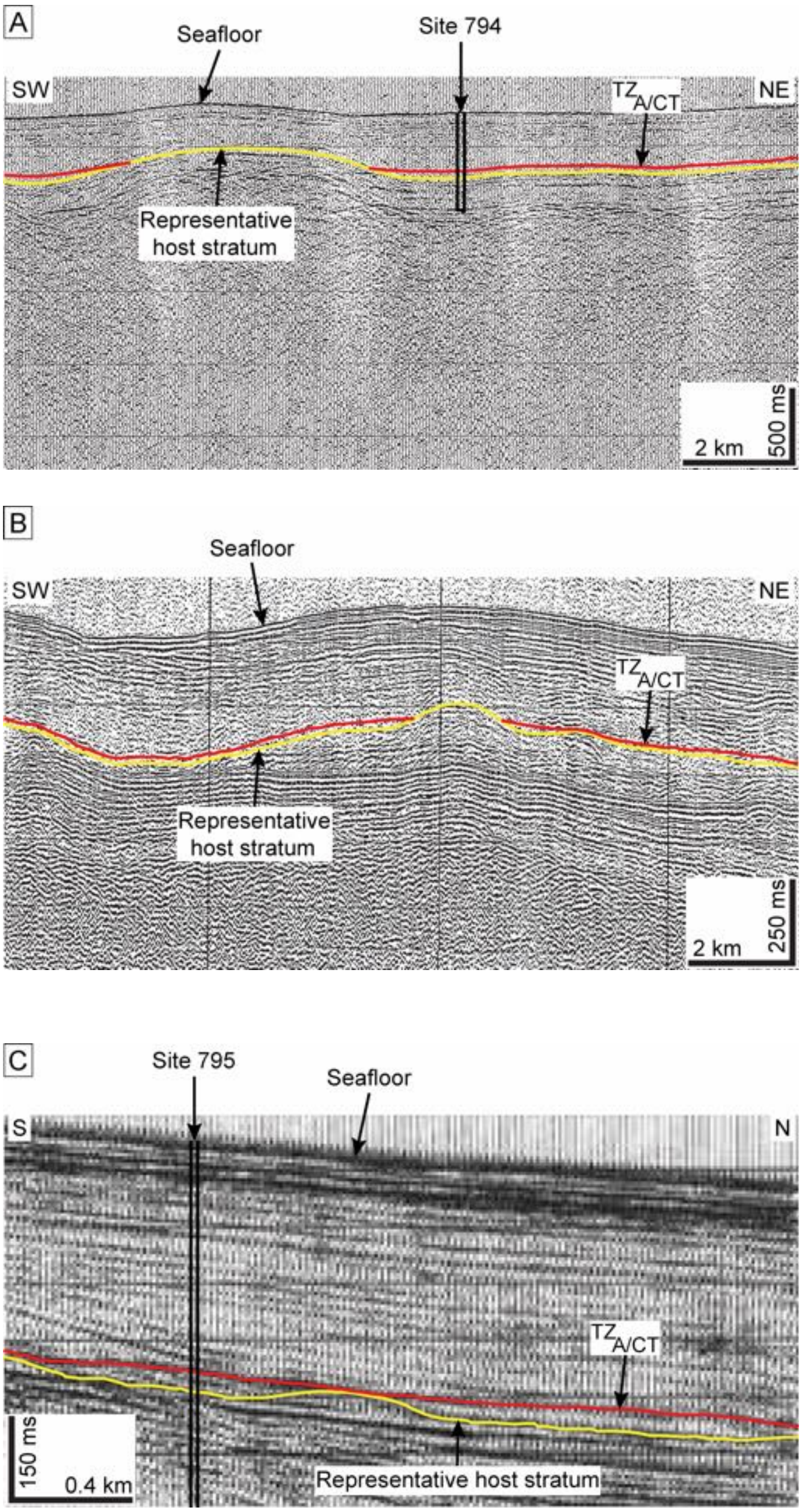

Figure 4: Likely active opal-A to opal-CT transition zone in the Sea of Japan represented by a seabottom-simulating reflector (modified from International Ocean Discovery Program Site Survey Data Bank, 2019). Note that the $TZ_{A/CT}$ cuts across the stratal reflectors, but mimicking the present-day seabed. A) A multi-channel seismic profile near Site 794 in the Yamato Basin. B) A seismic line mapped across the central part of the Yamato Basin. C) A single-channel seismic line over Site 795 in the Japan Basin.

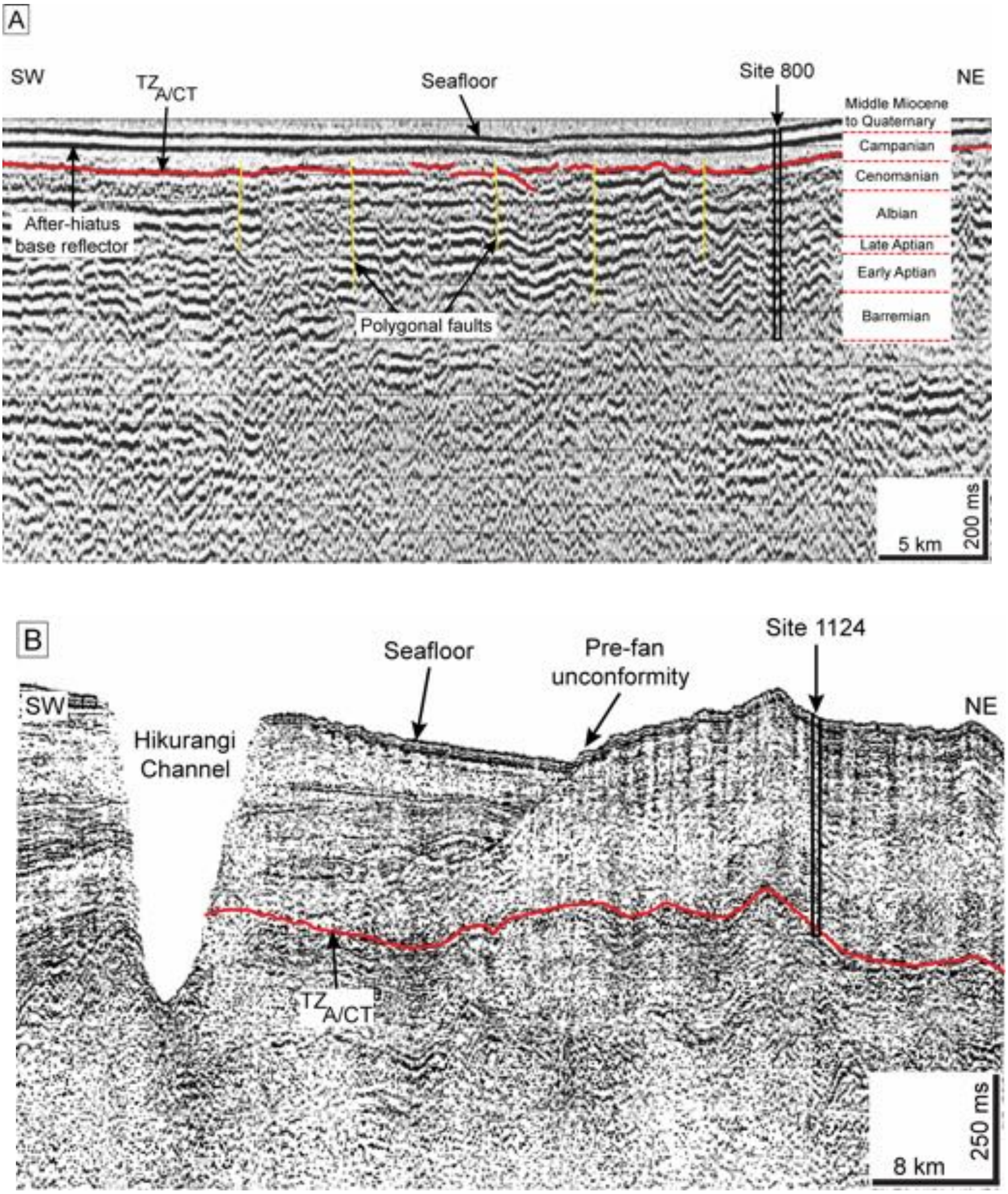

Figure 5: Likely arrested regional BSR opal-A to opal-CT transition zones. A) Cross-sectional seismic profile obtained on approach to ODP Site 800 from the western Pacific (modified from Shipboard Scientific Party, 1990c). The deformed shallow $TZ_{A/CT}$ mimics the overlying stratal reflection and the seabed. B) Seismic section hosting ODP Site 1124 in North Island, New Zealand (after Shipboard Scientific Party, 1999). Note that the deformed deep $TZ_{A/CT}$ lies parallel to the present-day seafloor.

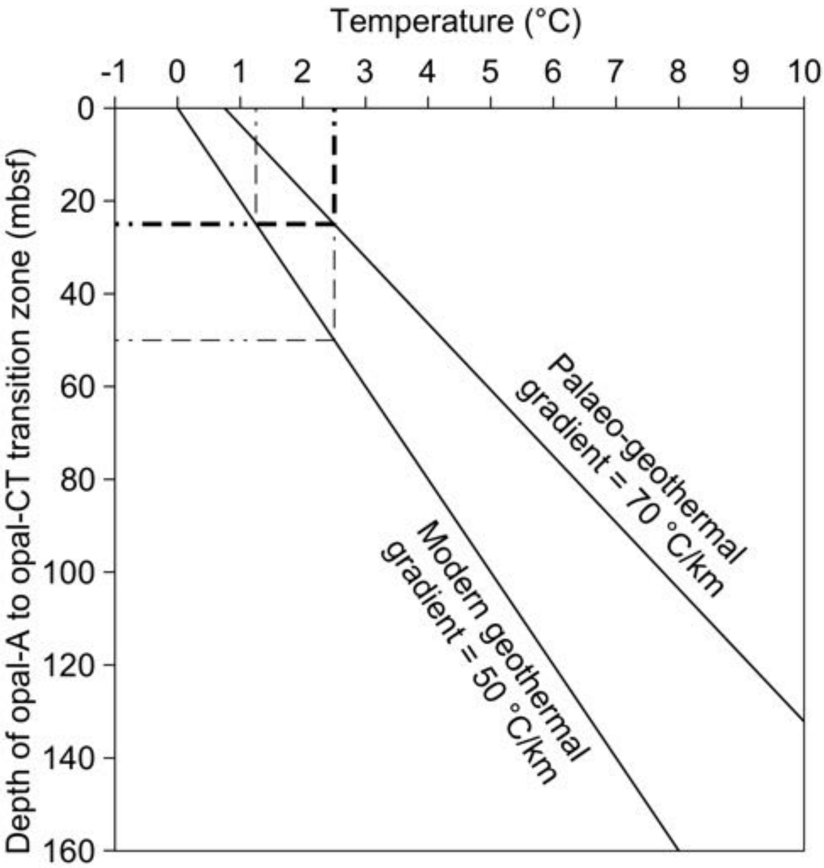

Figure 6: Present-day geothermal gradient and hypothetical palaeo-geothermal gradient at and in the vicinity of ODP Site 800 (drawn based on data from Shipboard Scientific Party, 1990c). Presently, the arrested $TZ_{A/CT}$ penetrated by this borehole lies at ~ 50 mbsf, where the temperature is 2.5 °C. The parallelism the $TZ_{A/CT}$ shows with the Middle Miocene after-hiatus base reflector suggests this reflector as the palaeo-seabed at that time (following Neagu et al., 2010b; also see Fig. 5A). The overburden above the $TZ_{A/CT}$ was therefore 20–30 m thick during the Middle Miocene, and the seafloor temperature was 0.75 °C. Given these depth and temperature constraints, a geothermal gradient of 70 °C/km was necessary for ongoing silica diagenesis during the Late Cretaceous to late Early Miocene.

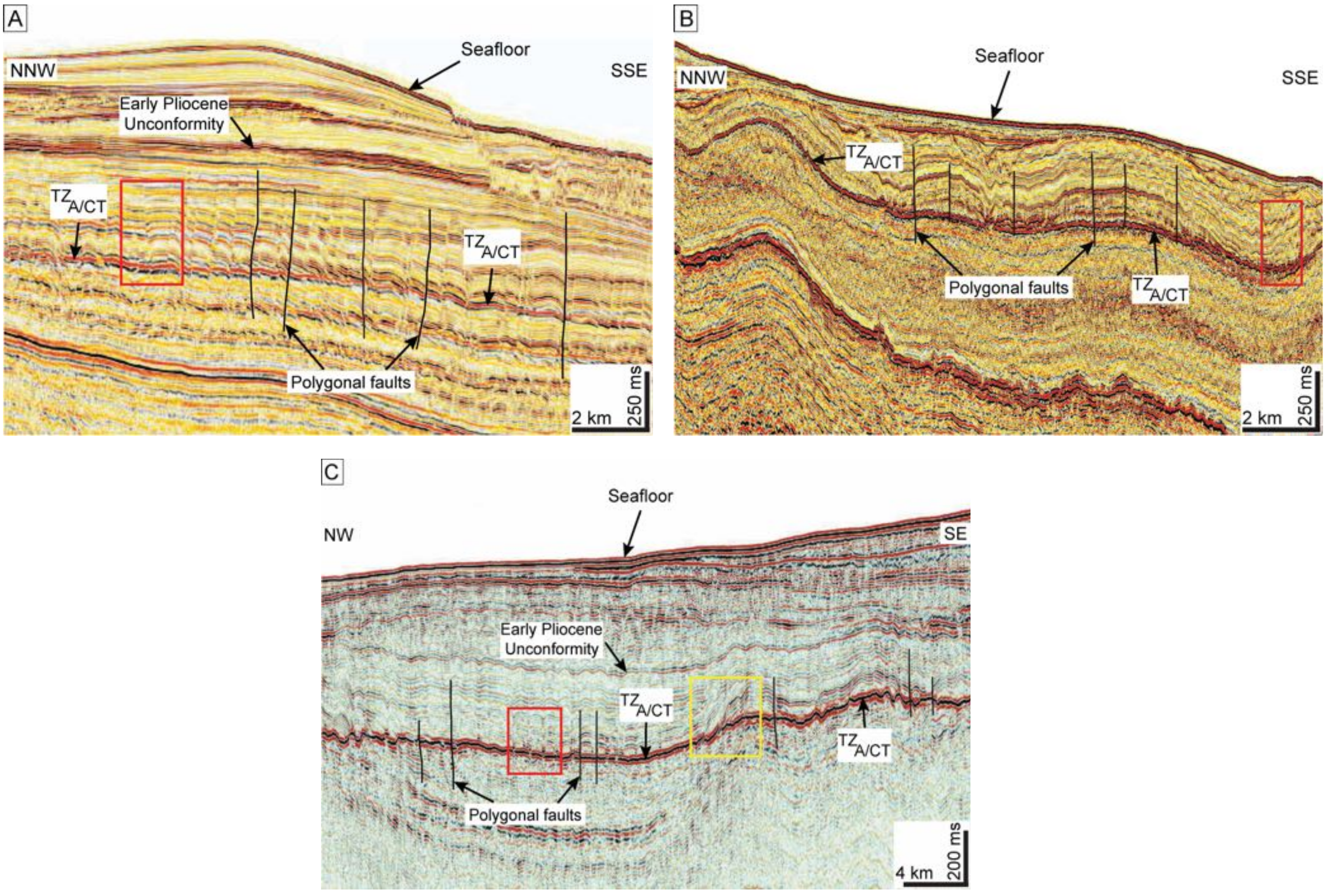

Figure 7: Association of silica diagenesis transition zones with various modes of deformation. A) A 3D seismic reflection section displaying the heavily faulted nature of the $TZ_{A/CT}$ from offshore Norway. Also seen is the ridge–depression structures at the $TZ_{A/CT}$, and the development of differential folds in the interval above it (red rectangle) (modified from Cartwright, 2007). B) Another 3D seismic profile from offshore Norway margin showing the $TZ_{A/CT}$ associated with polygonal faults, ridge–depression morphologies and their overlying folds (red rectangle), and anticlinal–synclinal structures (data courtesy of Statoil A/S). C) 2D seismic section from Faeroe-Shetland basin on the NE Atlantic margin showing the heavily deformed faulted/folded regional $TZ_{A/CT}$. The transition is also involved in ridge–depression structures (red rectangle) and serrated features (yellow rectangle) (modified from Davies and Cartwright, 2002).

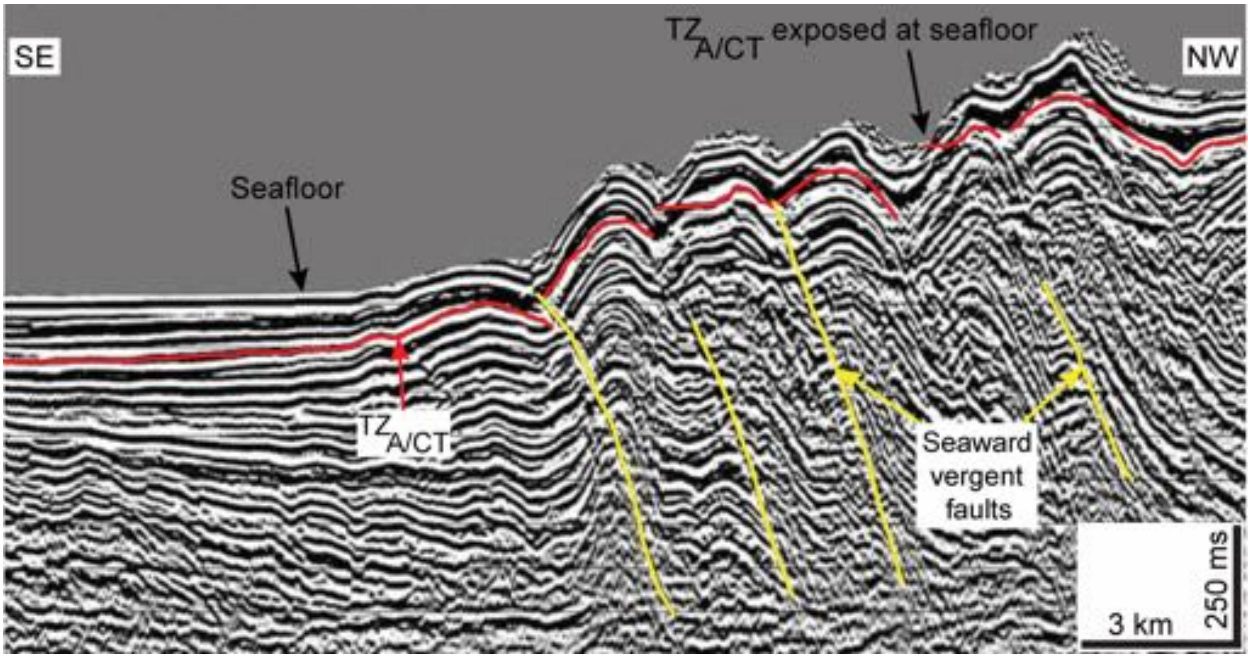

Figure 8: Seismic cross-sectional image from the Nankai Trough showing the truncation of $TZ_{A/CT}$ reflector at the eroded seafloor over the steep ridge slope (modified from McAdoo et al., 2004). Note the association of this arrested boundary with other modes of deformation, such as faults and regional folding.

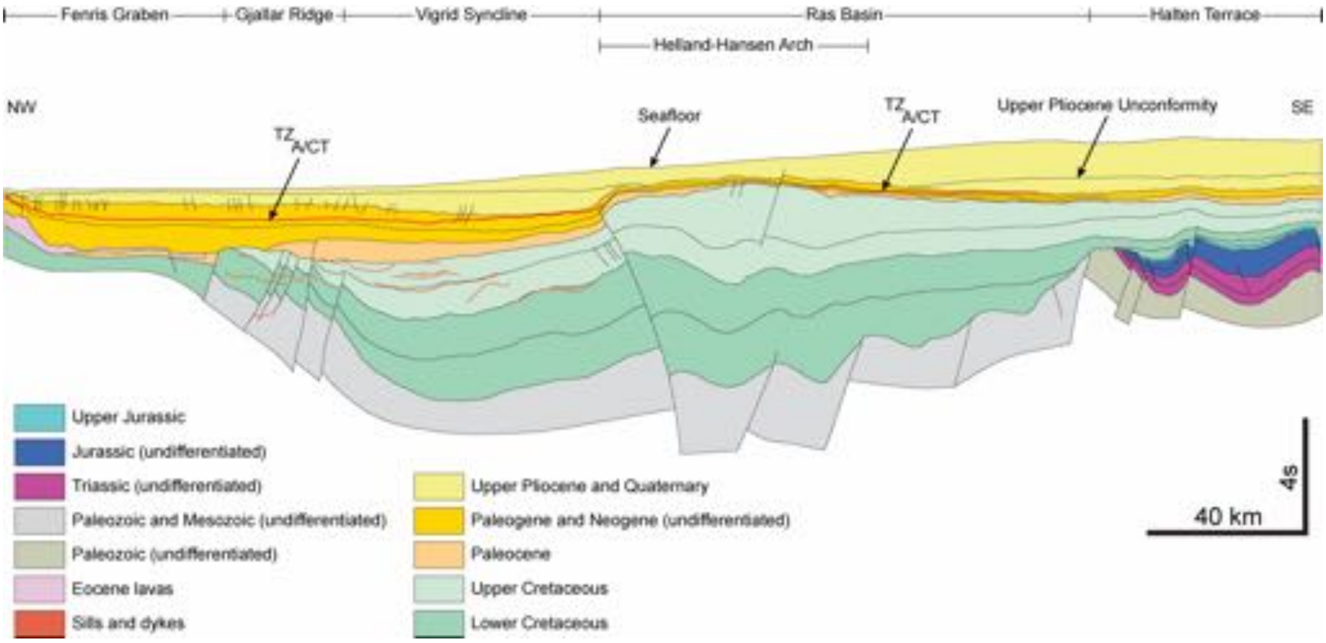

Figure 9: Geoseismic profile of Vøring Basin in the Norwegian Sea Continental Margin (redrawn and modified from Blystad et al., 1995). Note the non-BSR $TZ_{A/CT}$ (red line) cross-cutting domal nearby strata is itself involved in regional anticlinal—-synclinal structures, but roughly mimics the overlying Upper Pliocene Unconformity.

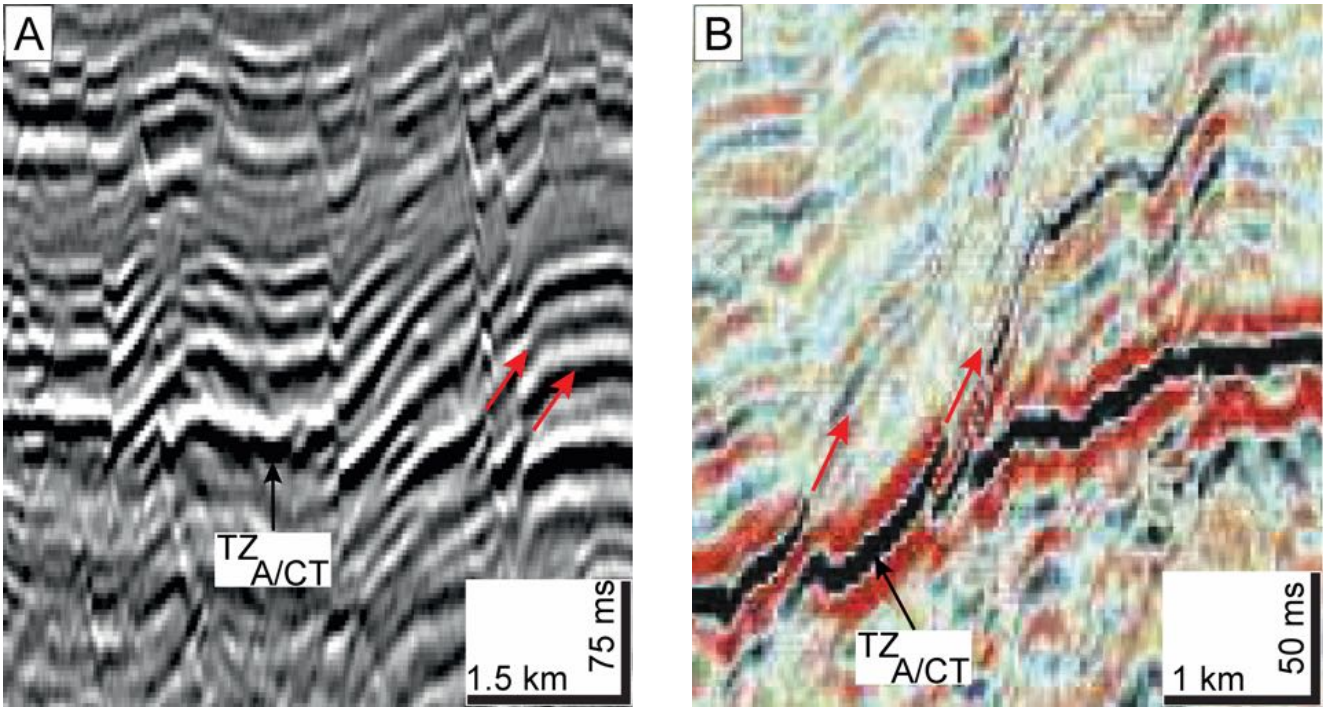

Figure 10: Serrated morphology in opal-A to opal-CT transition zones. A) Serrated pattern in the $TZ_{A/CT}$ from Møre Basin, mid-Norwegian margin. B) Close-up view of serrated feature in the $TZ_{A/CT}$ from Faeroe-Shetland basin (yellow rectangle in Fig. 7C).

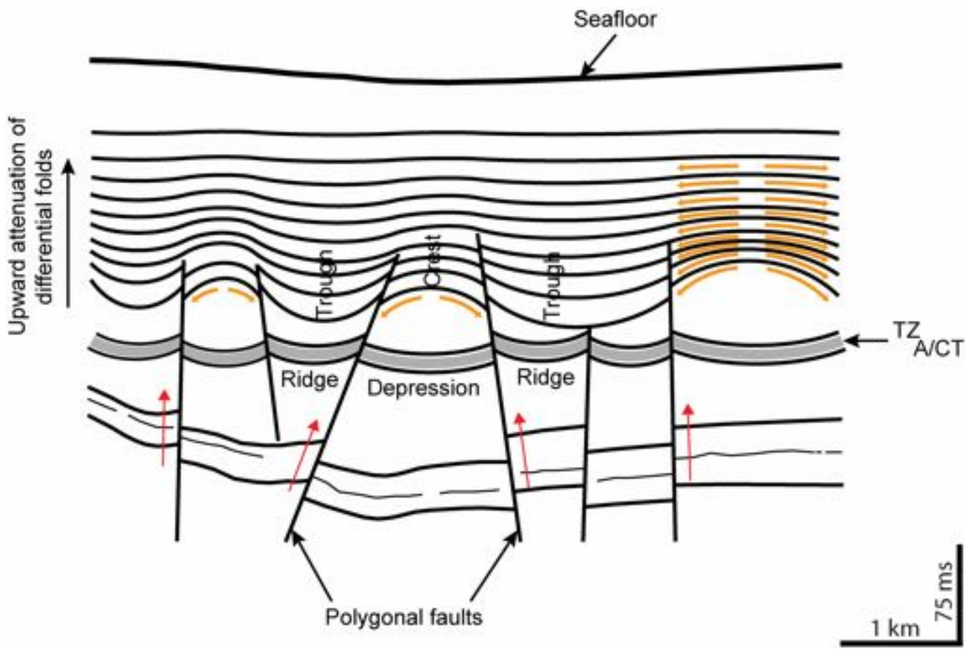

Figure 11: Sketch showing presumed pattern for the development of differential compaction folds above the $TZ_{A/CT}$ in the Neogene sediments of NE Atlantic margin. Orange curved arrows mark the direction of overburden porosity collapse. Red arrows along the polygonal faults denote the direction of hot-fluid flux. Note that the fold relief decreases upward in pace with the reduction in differential porosity collapse (orange arrows on the right side of the profile). The diagenetic state of the $TZ_{A/CT}$, however, cannot be confidently determined based on this model.

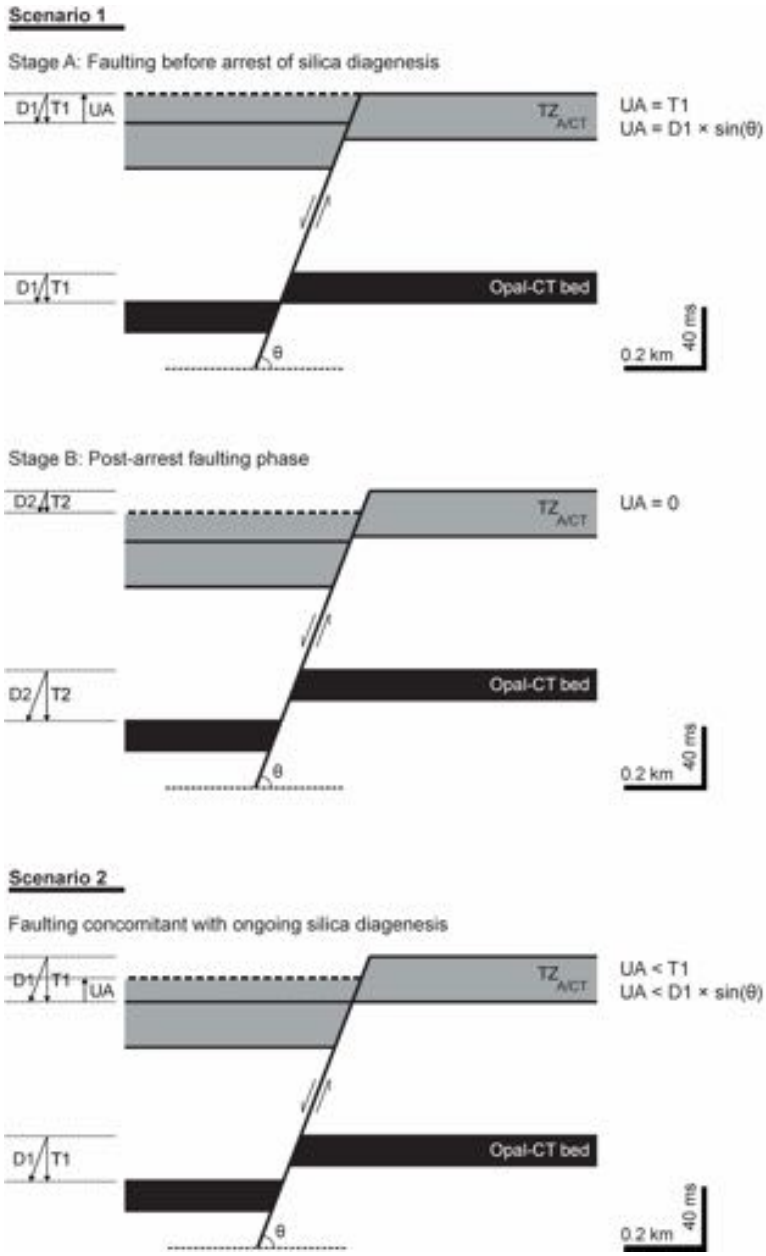

Figure 12: Presumed schemes of relationships between faulting and diagenetic state of the $TZ_{A/CT}$ in the Miocene deposits of NE Atlantic margin. The abbreviations represent: D1 = displacement along the fault during ongoing silica diagenesis, T1 = throw along the fault during ongoing silica diagenesis, UA = $TZ_{A/CT}$ upward advancement, D2 = displacement along the fault after arrest of silica diagenesis since Late Miocene, T2 = throw along the fault after arrest of silica diagenesis, and θ = fault dip angle.

Appendix I: The borehole sites used for drawing the isothermal curves in Figure 2. For every well, the vertical depth, the seafloor temperature, and the geothermal gradient are presented. Also listed is the depth of isotherms computed for five temperature layers, from 10 to 50 °C. Refer to Neagu et al. (2010b) for the geographic location of these boreholes.

Borehole site	Minimum distance from start point along NW–SE profile in Fig. 2 (km)	Borehole depth (mbsf)	Seabed temperature (°C)	Geothermal gradient (°C/km)	Isotherm (°C)				
					10	20	30	40	50
					Depth of isotherm (mbsf)				
6505/10-1	10.3	4319	0	35	286	571	857	1143	1429
6403/6-1	20.4	2374	-2.5	45	278	500	722	944	1167
6403/10-1	41.2	1656	-2	46	261	478	696	913	1130
6405/7-1	68.2	3000	-0.7	42	255	493	731	969	1207
6404/11-1	72.8	2130	-1	44	250	477	705	932	1159
6405/10-1	88.3	2231	-0.5	40	263	513	763	1013	1263
ODP 642	149.8	1229	0	40	250	500	750	1000	1250